Synthesis and Characterization of
Cerium (III) and (IV) Compounds

_____

A Thesis

presented to

the faculty of the Graduate School

at the University of Missouri – Columbia

_____

In Partial Fulfilment

Of the Requirements for the Degree

Master of Science

_____

by

Jason Ross

Dr. Justin Walensky, Thesis Supervisor

July 2022

Approval

The undersigned, appointed by the dean of the Graduate School, have examined the thesis entitled Synthesis and Characterization of Cerium (III) and (IV) Compounds, presented by Jason Ross, a candidate for the degree of Masters of Science, and hereby certify that, in their opinion, it is worthy of acceptance.

Professor Justin Walensky:
_____

Professor Wes Bernskoetter:
_____

Professor Heather Hennkens:
_____

Professor Craig Franklin:
_____

Success is not the key to happiness. Happiness is the key to success. If you love what you are doing, you will be successful.

Albert Schweitzer

Abstract

Department of Chemistry
University of Missouri

Master of Chemistry

by Jason Ross

Treatment of $Cp^*_2CeCl_2K$ with various aryl alcohols and amines produces $Cp^*_2Ce(O\text{-}2,6\text{-}iPr_2C_6H_3)$ and $Cp^*_2Ce(N(C_6H_5)_2)$. The crystallographic structures are presented as well as their fluorescence. Absorbance measurements provide unique absorbance maxima for each compound, however their fluorescence is exactly the same signifying that their molecular orbitals have similar energies. Treatment of $Cp^*_2Ce(O\text{-}2,6\text{-}iPr_2C_6H_3)$ with copper halide salts results in the formation of various Ce(IV)-halide compounds. Finally, in order to examine alternate ligand frameworks, other than Cp^*, treatment of $Ce(N(SiMe_3)_2)_3$ with H(esac) and H(Mes-Ph$_6$) resulted in unique cerium (III) complexes that contained β diketones. Within these complexes, their synthetic method and characterization are presented.

Acknowledgements

Contents

List of Figures

List of Tables

Hi Mom! Hi Dad!
*Waves**

Chapter 1

Introduction

1.1 The Lanthanide Series

As the periodic table orders elements according to varying atomic number, the lanthanides fall between barium (56) and halfnium (72). The lanthanides were some of the last elements to be discovered and although most viewed rare earth elements as uncommon, esoteric, and, as the name suggests, expensive, they have come to be invaluable to the technological advancement of our society. The discovery of the first rare earth elements, lanthanum and cerium, can be attributed to Mosander in 1840 CE. [1] It wasn't until roughly 100 years later when the remaining lanthanide elements were able to be successfully isolated and discovered. The reason for this long delay came from a series of misconceptions. For most of the history surrounding f-element chemistry, the lanthanides were considered to be uninteresting. During the early stages of investigation, the chemists in the field had no interest in studying these elements since they were considered to have no applicable foundation. More specifically, most constructed preconceived notions and viewed the lanthanides as just fancier versions of alkali or alkaline salts. [2]

Distaste in studying the lanthanide series came from the understanding that there was terrestrial scarcity - hence the name "rare" earth - regarding these elements. As seen in Table 1.1, the abundance of lanthanide greatly exceeds that of the transition metals. To put it in perspective, cerium, neodymium, and lanthanum are as common as cobalt and lead. Even more so, the least common lanthanide, thulium, has a greater abundance than most of the precious metals (Ag, Hg, etc). Despite some of these assumptions, the lanthanides still were able to earn their prestige with time.

TABLE 1.1: Abundance of Metallic Elements within the Earth's Crust (ppm). Table adapted from Wedepohl.

iron	43200	ytterbium	2.0
chromium	126	europium	1.3
cerium	60	molybdenum	1.1
nickle	56	tungsten	1.0
lanthanum	30	holmium	0.80
neodymium	30	terbium	0.65
cobalt	24	lutetium	0.35
lead	14.8	thulium	0.30
praseodymium	6.7	silver	0.07
samarium	5.3	mercury	0.040
gadolinium	4.0	gold	0.0025
dysprosium	3.8	platinum	0.0004
erbium	2.1	rhodium	0.0004

The lanthanide series has been extremely beneficial for our society as they have found great applications as phosphors [3], optical coatings [4], Pb^{2+}-free alternatives [5], and catalysts [6].

1.2   Electronic Structure of the Lanthanides

With the lanthanides, orbital energies behave slightly differently than the rest of the periodic table. The first difference can be noticed as orbital energies start to change as more protons are added to each element across the row. As seen in Table 1.2, lanthanum's 5d orbital is found to be lower in energy than the 4f, so the electronic configuration is [Xe] $6s^2$ $5d^1$ From here, as more protons are added to the nucleus, the 4f orbitals contract and become more stable than the 5d. Cerium has an electronic configuration of [Xe] $6s^2$ $5d^1$ $4f^1$ and this trend continues with Pr being [Xe] $6s^2$ $5d^1 4f^3$. This pattern continues for Nd-Eu. After europium, the stability of the half-filled f-orbital, an electron is added to the 5d orbital. Gd has an electronic configuration of [Xe] $6s^2$ $5d^1$ $4f^9$. After Gd the pattern is then resumed leaving the last lanthanide Lu, to have an configuration [Xe] $6s^2$ $5d^1$ $4f^{14}$.

1.2.1   Lanthanide Contraction

Traditionally, for elements that have more than one electron, decreasing atomic radii with an increase in nuclear charge tends to be offset by an increase in electrostatic repulsion within the electron cloud. For the lanthanides (La-Lu), as the atomic number increases, an electron is not added to the outer shell, but rather an inner 4f shell. To

TABLE 1.2: Electron configuration of the lanthanide and their common oxidation state

Element	Atom Configuration	Ln $^{3+}$
La	[Xe] $5d^1 6s^2$	[Xe]
Ce	[Xe] $4f^1 5d^1 6s^2$	[Xe] $4f^1$
Pr	[Xe] $4f^3 6s^2$	[Xe] $4f^2$
Nd	[Xe] $4f^4 6s^2$	[Xe] $4f^3$
Pm	[Xe] $4f^5 6s^2$	[Xe] $4f^4$
Sm	[Xe] $4f^6 6s^2$	[Xe] $4f^5$
Eu	[Xe] $4f^7 6s^2$	[Xe] $4f^6$
Gd	[Xe] $4f^7 5d^1 6s^2$	[Xe] $4f^7$
Tb	[Xe] $4f^9 6s^2$	[Xe] $4f^8$
Dy	[Xe] $4f^{10} 6s^2$	[Xe] $4f^9$
Ho	[Xe] $4f^{11} 6s^2$	[Xe] $4f^{10}$
Er	[Xe] $4f^{12} 6s^2$	[Xe] $4f^{11}$
Tm	[Xe] $4f^{13} 6s^2$	[Xe] $4f^{12}$
Yb	[Xe] $4f^{14} 6s^2$	[Xe] $4f^{13}$
Lu	[Xe] $4f^{14} 5d^1 6s^2$	[Xe] $4f^{14}$

more appropriately visualize the spacing's of orbitals within a lanthanide, Figure 1.1 depicts the the radial distribution functions of 4f, 5s, 5p, and 6s electrons for a generic lanthanide.
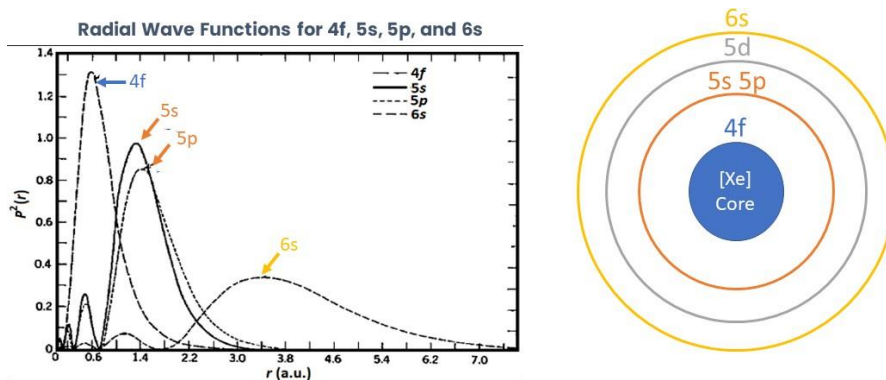
FIGURE 1.1: Radial distribution functions of 4f, 5s, 5p and 6s electrons for a generic lanthanide. Figure adapted from Wiley.[7]

As electrons are added to the 4f shell, shielding effects that occur are only partial to what they would normally be as a result of their diffusive property within the orbital. As demonstrated in Figure 1.2, as you move across the row the radius of the lanthanide ions decrease gradually as the atomic number increase. This results in constant changes

in properties to change at a regular and consistent pattern as you go across the row. For example, as atomic number increases across the row the stability constant increases.[8]
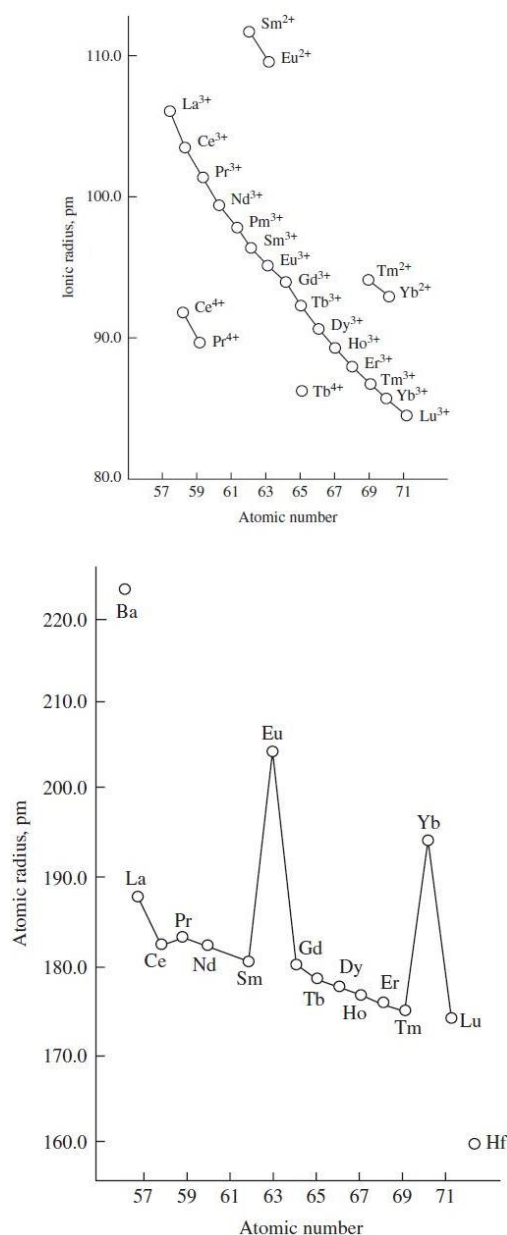
FIGURE 1.2: Decreasing ionic radii (top) and decreasing atomic radii (bottom) compared with the atomic number of the lanthanide series. Figure adapted from Huang.[9]

Within the decrease of radii, the unusual behavior of Ce, Eu and Yb can be explained. Since the atomic radius of a metal is equivalent to the maximum radii of of the outermost electron cloud density, the maxima of orbital radii overlap which allows electrons to move freely. These electrons are what are known as conducting electrons.[10] Within lanthanide metals, there are three conducting electrons. As a result of Hunds rule, Yb and Eu maintain a $4f^7$ and $4f^{14}$ electron configuration while providing only two conducting electrons. Trivalent cerium has only one 4f electron and yet it provides

four conducting electrons to obtain a stable electronic configuration. Given that the lanthanide series are the only row of elements that contain a radii contraction across the series, this advantageous trait enables control of reaction pathways.[11]

	Metal Radius	Yield of Hydride Product	Reaction Time
(C5H5)2ErMe(THF)	1.004	55%	24 h
(C5H5)2YbMe(THF)	0.985	< 1%	24 h
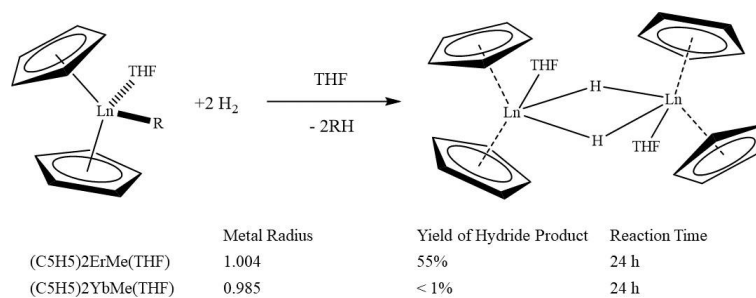
FIGURE 1.3: Sensitivity of Hydrogenolysis Reactivity to the Metal Center. Figure adapted from Evans.[2]

The magnitude and effect of the altercation of the metal center is displayed in Figure 1.3. By changing the size of the metal center, a 0.02 Å difference can drastically impact the reaction.

1.3 Ionization Energies of the Lanthanides

As was mentioned in the previous section, the general electronic configuration for the lanthanides is [Xe] $6s^2 5d^0 4f^n$. The exceptions to this rule are La, Ce, Gd and Lu. In this case, for La, and Ce, the 4f orbital has not contracted enough to allow the 5d orbital to become more stable. For Gd and Lu, Hunds rule dominates by making a half or full filled shell more stable.

As these metals form ions these electronic configurations change as electrons are removed from the 6s and 5d orbitals. In doing so the trivalent oxidation state dominates. As these atoms ionize their ionization potentials follow the general pattern where the next ionization pattern will be greater than the previous one.

$$I_4 > I_3 > I_2 > I_1$$

As electrons are removed there is an increase in positive charge which allows for greater electrostatic interaction. These values and trend are demonstrated in Table 1.3 and Figure 1.4.

TABLE 1.3: Ionization energies of the lanthanide series

	I_1	I_2	I_3	I_4	$I_1 + I_2$	$I_1+I_2+I_3$	$I_1+I_2+I_3+I_4$
La	538	1067	1850	4819	1605	3455	8274
Ce	527	1047	1949	3547	1574	3523	7070
Pr	523	1018	2086	3761	1541	3627	7388
Nd	529	1035	2130	3899	1564	3694	7593
Pm	536	1052	2150	3970	1588	3738	7708
Sm	543	1068	2260	3990	1611	3871	7861
Eu	546	1085	2404	4110	1631	4035	8145
Gd	593	1167	1990	4250	1760	3750	8000
Tb	564	1112	2114	3839	1676	3790	7629
Dy	572	1126	2200	4001	1698	3898	7899
Ho	581	1139	2204	4110	1720	3924	8034
Er	589	1151	2194	4115	1740	3934	8049
Tm	597	1163	2285	4119	1760	4045	8164
Yb	603	1176	2415	4220	1779	4194	8414
Lu	523	1340	2033	4360	1863	3896	8256
Y	616	1181	1980	5963	1797	3777	9740

Moving across the lanthanide series there are a few noteworthy trends. First, upon moving across the row one it is evident that there is an increase in ionization energy across the row. While one might hypothesize that, because of the lanthanide contraction across the row, a more consistent pattern would be apparent, in actuality a more inconsistent pattern forms. Upon examination of the I_3 ionization energies, most elements fall
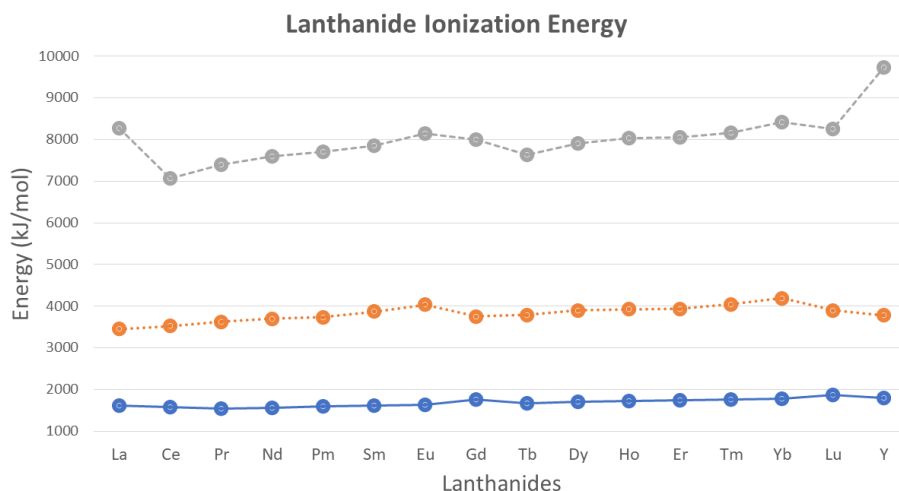
FIGURE 1.4: Graph of the added ionizaiton potentials across the lanthanide series. Dashed(Grey) = I1 + I2 + I3 + I4, Dotted (Orange) = I1 + I2 + I3, Line (Blue) = I1 + I2

within a range of 2100 - 2400 kJ/mol. The low energies for Gd and Lu are result from their electron configuration where an electron (See Table 1.2) is taken from the d orbital instead of the f orbital. The high I3 values for Eu and Yb stem from the stabilizing effects of the half and full filled orbital. These trends are better observed in Figure 1.4 where the +2, +3 and +4 oxidation state can be visualized across the entire row. Upon examining the 4th ionization potentials, cerium is observed to have the lowest energy allowing this oxidation state to be the most accessible.

1.4 Cerium Chemistry

As mentioned previously, the lanthanides have the tendency to form various oxidation states. Cerium is one of the lanthanides with an accessible +4 oxidation state. Only cerium (IV) is stable in solution as a result of its extremely low Ce(IV)/Ce(III) potential. [12] Due to interchangeable oxidation state, it is of great interest to syntheses Ce-based compounds that can include both oxidation states.

Cerium (IV) exhibits incredibly different reactivity from the other rare earth elements. Ce(IV) will begin to form hydrates in extremely acidic environments while others will hydrolyze in more neutral conditions. Additionally, cerium is able to form stable complexes with F^- and O^{2-} in various acidic media. Stability calculations surrounding Ce^{4+} and F^- demonstrate the stability between Ce-F complexes. For example, the stability constants for $[CeF^{3+}]$, $[CeF_2^{2+}]$, $[CeF_3^+]$, and $[CeF_4]$ are 10^7, 10^{14}, 10^{20}, 10^{24} within perchloric acid medium. Additionally, Ce^{4+} and F^- are able to forms stable complexes

of [CeF$_2^{2+}$] and [CeF^{3+}] in sulfuric acid. [13,14] As a result of these studies, developing new Ce(IV)-F complexes helps to gain a better understanding of the stability of Ce(IV) in solution. [15]

Currently within the literature there exists a variety of Ce(III) complexes that have been synthesized. However, in comparison with the other lanthanides, the high oxidation potential for Ce(IV) has limited the reaction chemistry surrounding the element. Given that, success has been achieved by taking advantage of the lanthanides high oxophilicity and saturation of the coordination sphere. Three examples shown in Figure 1.5 demonstrate utilization of Cp* ligands, siloxide ligands, and demonstrate the oxidative chemistry needed to synthesize various Ce(IV) compounds.
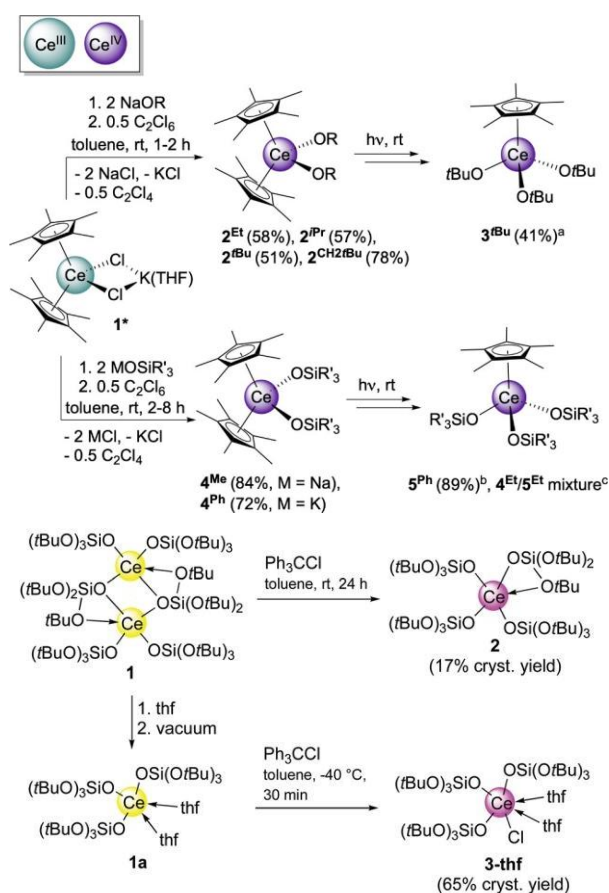
FIGURE 1.5: (Top) Reaction pathway to cerium(III) and (IV) complexes. (Bottom) Reaction pathway of cerium siloxide(III) complexes reacting with Ph$_3$CCl to form cerium(IV) compounds. Figures adapted from Anwander [16,17]

Cerium(IV) compounds that contain aryloxides are of interest due to their applications as molecular precursors to cerium oxide materials. In an attempt to bolster the compounds thermal stability, oxygen based donors, as well as bulky moieties, are utilized and, as demonstrated in Figure 1.6, series Ce(IV) compounds containing aryloxide and alkoxide ligands now are known to exist within the literature. In addition to the Cp and Cp*

compounds, the Walensky group seeks to present another ligand framework that contains great potential. This framework is the β-diketone framework.
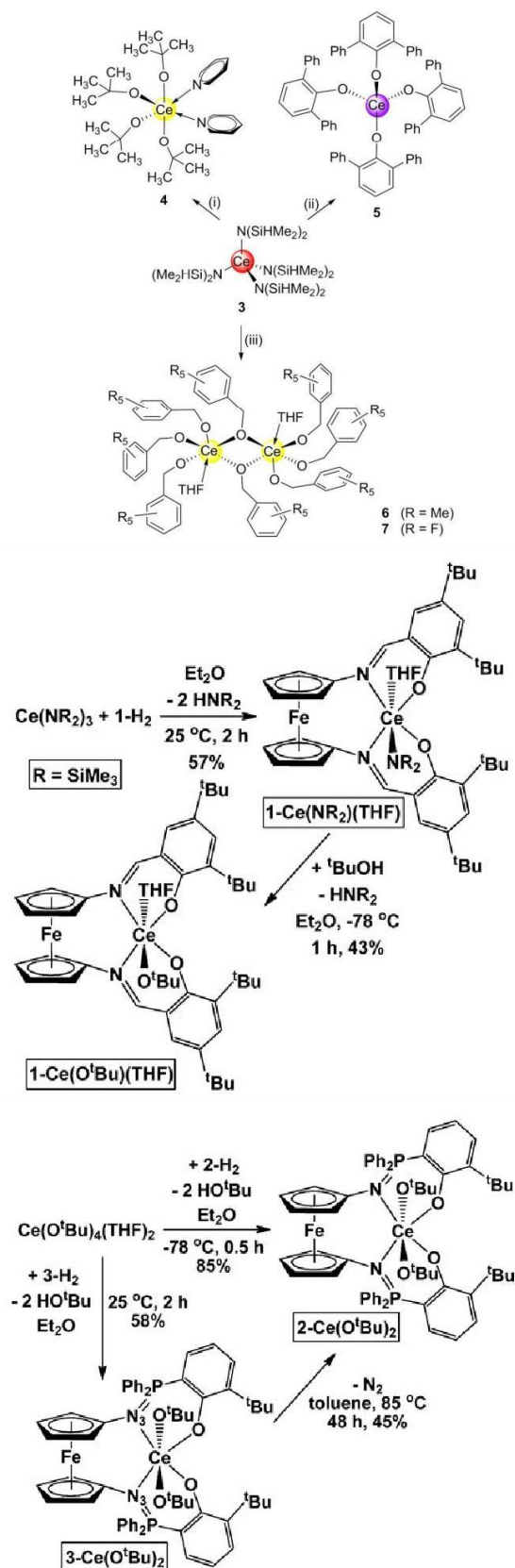
FIGURE 1.6: Top: Synthesis of various Cerium (III) and (IV) compounds from Cerium (IV) amide. Figure adapted from Schelter[18] Bottom: Reaction scheme of various heteroleptic cerium complexes that are supported by ferrocene based chelating agents. Figures adapted from Diaconescu[19]

β diketones are another widely investigated ligand within lanthanide chemistry. They are most commonly found as prototropic tautomerisms, also known as keto-enol tautomerisms, in both solutions and solids. Evidence for this stems from ^{1}H NMR and single crystal X-ray diffractometry. An example is demonstrated in Scheme 1.1. A β diketones acts as a monobasic acid since the enol proton can be readily deprotonated. As a result of this, the β diketone can act as a monoanionic O-O bidentate ligand when coordinating to a lanthanide ion. In a similar fashion to the tris Cp ligand, tris(β diketonates) can also exist. These complexes are electrically neutral and can dissolve in various organic solvents such as chloroform, benzene and pentane.
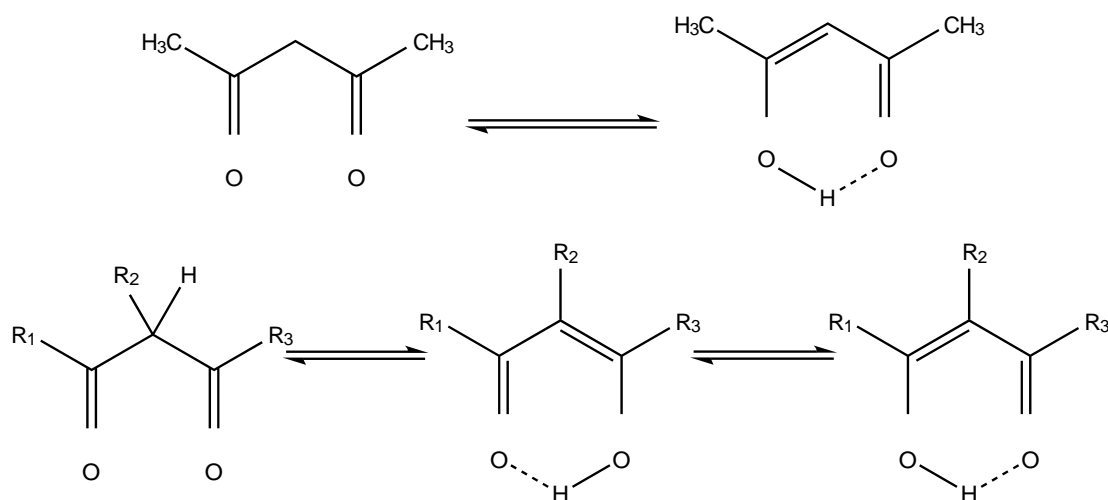
SCHEME 1.1: Depiction of the keto-enol tautomerism equilibrium in acetylacetone (top). Keto-enol tautomerism equilibrium of acetylacetone derivatives (bottom). Figure adapted from Huang. [9]

Aside from the academic and catalytic potential they have, β diketones have been utilized in the refining of metals, separation of lanthanides, depositing of thin films. Current areas of research regarding β diketones include CVD applications [20], single molecule magnets [21], luminescent compounds such as OLEDs, and molecular sensing. [22]

In synthesizing β diketones, the Claisen condensation reaction is the primary synthetic route most commonly used. [23,24] As seen in Figure 1.7, the primary reaction involves either two or one ester and another carbonyl in the presence of a strong base which will produce a β diketone and an alcohol. For most of the 1940's, and as shown in Figure 1.7, variations of β diketones used simple alkyl or phenyl substituent. It wasn't until 1944 when dipivaloylmethane (dpm) was used and its success catalyzed the exploration of hindered β diketones. While there have been numerous other novel synthetic methods of various derivatives, this report focuses on the development and process of sterically hindered β diketones developed by Marshak in 2017. [25–27]
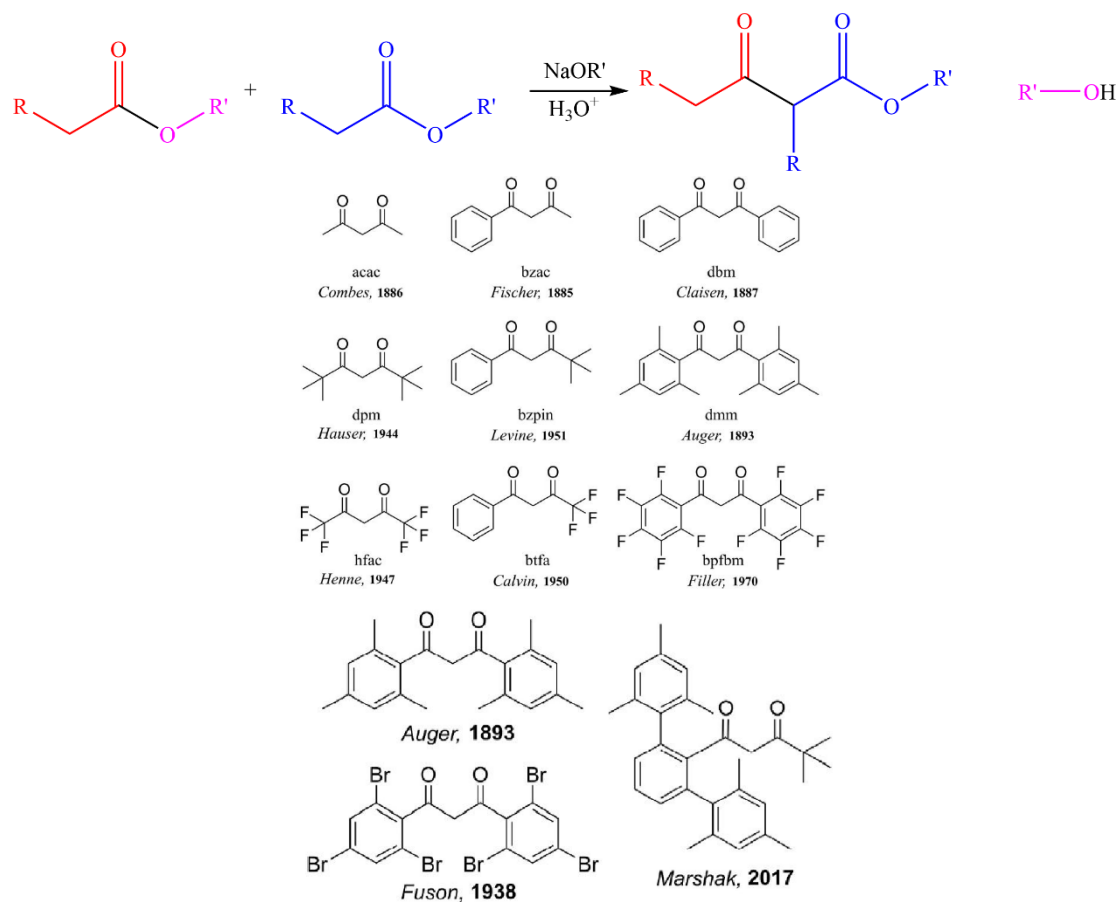
FIGURE 1.7: Top: Reaction scheme for the synthesis of β dikeytones. Middle: current diketones within the literature Bottom: Recent sterically hindered β diketones. Figure adapted from Marshak.[28]

To date, no lanthanides are reported with the use of sterically encumbered β diketones however, current literature for lanthanides β diketonates within rare earth separation and luminescence is flourishing. β diketones have been found to be extremely effective in separating chemical mixtures which is extremely advantageous in expanding the availability of the elements.[29,30]
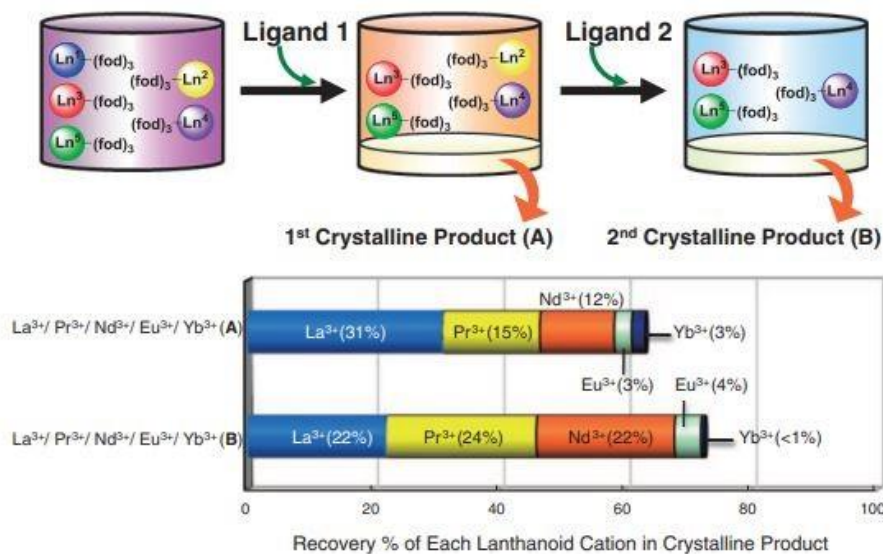
FIGURE 1.8: Step-wise separation profiles of five lanthanide tris(β-diketonates) mixture. [Ln(fod)$_3$] (Ln = La^{3+}, Pr^{3+}, Nd^{3+}, Eu^{3+}, and Yb^{3+}) = 2 at 102 M each, [Ligand] = 1 at 102 M. Figure adapted from Tsukube[29]

Additionally, utilization of the ligand has been found to amplify luminescent emissions of lanthanides. Within the recent decade, metal complexes of lanthanide ions with light harvesting organic chromophores have received great attention. While the first amplified emission of Eu^{III} complex was observed in 1492,[31] a paper examining the isostructural series M^{III}(L)$_3$(diglyme) (where M = La, Ce, Pr, Sm, Eu, Gd, Er, Lu) can act as second-order nonlinear optical chromophores as a result of their unpaired f-electrons.[32] In a similar manner, a series of liquid crystalline M^{III}(β diketone)$_3$ (M = La, Eu, Tb, Dy, Ho, Er, Tm, and Gd) were able to be synthesized using aliphatic ligands that contained cyclohexyl and n hexyl substituents.

Within the literature, Marshak was able to find that utilization of a sterically encumber m-terphenyl ligand, H(esac), blocked the formation of the more stable M^{III}(esac)$_3$ complex and instead forms M^{III}(esac)$_2$Cl (M = Ti, V, Cr).[28] Within this report, the development of similar compounds that contain cerium is of focus.

1.5 Luminescence and Fluorescence in Cerium compounds

Within luminescence of the lanthanide series, there exists unique properties. The energy level diagram for all the Ln^{3+} species can be found in Figure 1.9. This data is based on theoretical predictions that is combined with experimental results.

13
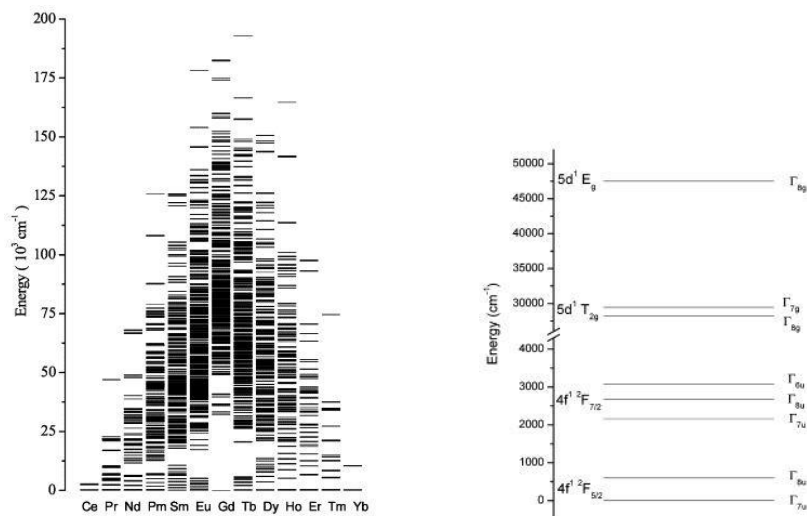
FIGURE 1.9: (Left) Energy level for all the Ln[3+] species. Figure adapted from Burdick[33]. (Right) Energy level diagram of Ce[+3] ion with extended 5d orbitals to denote excitation's to higher levels. Figure adapted from Barandiara[34].

In the lanthanides, the outer 5s and 5p orbitals provide the 4f orbitals efficient shielding from any nearby ligands on a lanthanide complex. As a result of this, there is extremely low crystal field splitting effects (roughly on the order of 100 cm⁻¹). [35] In terms of absorbance, most lanthanides absorb electromagnetic radiation within the visible region. This is result from excitation of the ion from its ground state to a higher electronic state as a result of the partially filled 4f subshell. The f-f transitions that occur can be excited in two ways: by magnetic dipole and electric dipole radiation. While the electric dipoles are often found to be extremely weak in lanthanides, within fluorescence spectra, the magnetic dipole transitions can often be seen. Magnetic dipole transitions are parity-allowed while electric dipole transitions are parity forbidden (otherwise considered Laporte-forbidden). The f-f transitions gain their intensity through interactions with higher electronic state that exist in opposite parity. This can occur through either the effects of a low symmetry ligand field (permanent) or through asymmetric molecular vibrations that may remove any center of symmetry within the molecule. This process is known as vibronic coupling. [36]

Within the lanthanide series, not all lanthanides provide f-f transitions such La and Lu which contain f^0 and f^{14} electronic configurations. For cerium the single $4f^1$ electron, there exists no f-f transitions as a result of there being no upper state with a single L-quantum number. In terms of the two bands seen in Figure 1.9, the transitions occur between the $^2F_{5/2}$ and $^2F_{7/2}$ only within the infrared region and are usually viewed as a broad band around 2000 cm⁻¹. Within the visible region, Ce(III) species do give rise to a broad $4f^n$ to $4f^{n-1}5d^1$ transition such as those depicted in Figure 1.9

Additionally, many lanthanides exhibit luminescence and will emit radiation from an excited electronic state. The general process is presented in Figure 1.10.
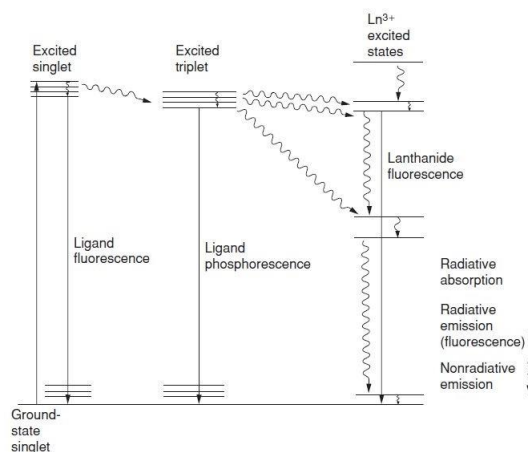
FIGURE 1.10: General fluorescence pathway in lanthanides. Figure adapted from Cotton [35]

In terms of cerium, with its split energetic states being extremely close together, most UV-vis and fluorescence spectra will provide a single peak that contains a shoulder. This denotes that a doublet is common since there should be transitions from the lowest 5d excited state to the spin-orbit split 4f ground state that is split by spin-orbit interaction into two sublevels ($^2F_{5/2}$ and $^2F_{7/2}$). [37] The energy between levels at the bands is known to be quite close. As an example, when cerium has been investigated as a phosphor, the data gathered during these experiments is demonstrates this property.
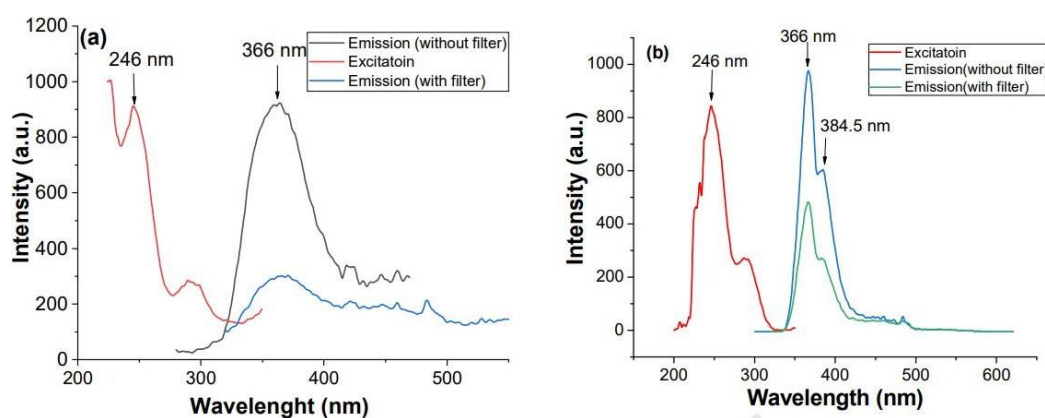
FIGURE 1.11: (a and b)Emission and excitation spectra of Ce-incorporated phosphor presented in a manuscript written by Kessler [38]

As presented in Figure 1.11, the emissions data in both graphs depicts a doublet that occurs as the electron is transitioning from the lowest 5d excited state to both of the 4f ground states.

1.6 Plan of Research

The ultimate goal of this this thesis is to further expand the chemistry behind Ce(III) and Ce(IV) complexes. Cerium has gained considerable attention as a result of the long standing interest to create earth-abundant and inexpensive photo-catalysts, utilize its high availability and explore its reversible redox chemistry. Despite the large amount of Ce(IV) complexes, organocerium complexes that contain Ce(IV) with cyclopentadineyl ligands are quite rare. [39,40] The coordination environment around the metal center plays an important role when stabilizing Ce(IV) species and will be explored within this thesis. Recently, the Anwander group reported a Ce(IV) metallocene $Cp^*_2CeCl(O\text{-}2,6\text{-}iPr_2C_6H_3)$ from the insitu reaction of $(C_5Me_5)_2CeCl_2K(THF)$ with $NaO\text{-}2,6,^iPr_2C_6H_3$ and a half equivalent of hexachloroethane. [16] This thesis proposes an alternative route to synthesizing similar Ce(IV) complex's. Given the strong electronegativity of fluorine and the high electropositive nature of cerium, effort will also be focused on creating a Ce(IV)-F metallocene. Finally, with Cp^* metallocene framework being a staple within organometallic chemistry, efforts are also focused on developing a new ligand framework that can undergo identical reactivity. As such, sterically encumber β diketones are utilized to form various Ce(III) complexes.

Chapter 2

Synthesis Structure and Optical Properties of Cp*$_2$Ce^{III}-X

2.1   Introduction

In utilizing cheap and abundant lanthanide based photocatalysts, there presents an opportunity to replace those that currently use precious metals. It is known that the luminescence of Ln(III) ions is affected by its atomic environment, specifically regarding the sterics surrounding the element. In exploring this field, luminescence can be used to detect particular molecules or to label them for imaging of living cells. In more advance cases, applications involve cancer identification and other biomedical diagnosis. [41–45] Attention is focused on cerium as a result of the doublet 4f to 5d excitation and emission. Herein, the goal is to explore the photophysics of the Ce(III) ion within different atomic environments .

Additionally, it is also important to mention within organolanthanide compounds that there stands a belief that there exists significant degree of covalency that stems from use of 5d orbitals. Previous studies include the luminescence of Cp$_3$Tb, Cp$_2$TbX, and TbCl$_3$ complexes, as well as Cp$_3$Yb, (C$_5$Me$_5$)$_2$Eu, and (C$_6$Me$_5$)$_2$Yb complexes which demonstrated that the observed luminescence at various energies was lower than would be expected for truly ionic compounds. [38] This decrease was attributed to the potential for some covalent character to be at play within these compounds. Recently, it was reported that a Ce(III) compound, Cp*$_2$CeCl$_2$Li, compound demonstrated strong luminescence in the solid state at room temperature. [46] Trivalent cerium is known to have a low excited state 4f^{0}5d^1 and compounds that utilize this metal should represent a better test of its trivalent covalent character.

2.2 Materials and Methods

All syntheses were carried out under an N_2 atmosphere using glovebox and Schlenk techniques unless otherwise stated. All non-deuterated solvents used were dried by passing through a solvent purification system (MBraun, USA) and stored over sieves, and potassium metal for aromatic and aliphatic solvents or calcium hydride for ethereal solvents.Cp*K[47], Cp*$_2$CeCl$_2$K[48], and Cp*$_2$CeN(SiMe$_3$)$_2$ [49], was prepared accordingly to their literature procedures. Benzene-d6 (Cambridge Isotope Laboratories) was degassed by three freezepumpthaw cycles and stored over molecular sieves. All ^{1}H spectra were taken on 600 MHz or 300 MHz Bruker spectrometers. All NMR chemical shifts are reported in ppm. ^{1}H NMR chemical shifts were referenced internally to the residual solvent peaks. IR spectra were recorded on a Nicolet Summit Pro FTIR spectrometer using a KBr pellet. Electronic absorption measurements were recorded in a sealed 1 cm quartz cuvette with a Varian Cary 5000 UVvisNIR spectrophotometer. Elemental analysis was performed on a Carlo Erba 1108 elemental analyzer, outfitted with an A/D converter for analysis using Eager Xperience software. SCXRD data was measured on a Bruker SMART diffractometer with an Apex II area detector (Bruker AXS LLC, USA) using Mo K radiation from a sealed source with focusing optics or collected on a Bruker D8 Venture with a Photon 100 CMOS area detector (Bruker AXS) using Mo K radiation from a microfocus source. Collection temperatures were controlled using Cryostream 700 and 800 cryostats (Oxford Cryosystems, UK). Hemispheres of data were collected using strategies of scans about the omega and phi axes. The Bruker Apex3 software suite was used for unit cell determination, data collection, and data reduction.

2.2.1 Synthesis of Cp*$_2$Ce(O-2,6-iPr$_2$C$_6$H$_3$)
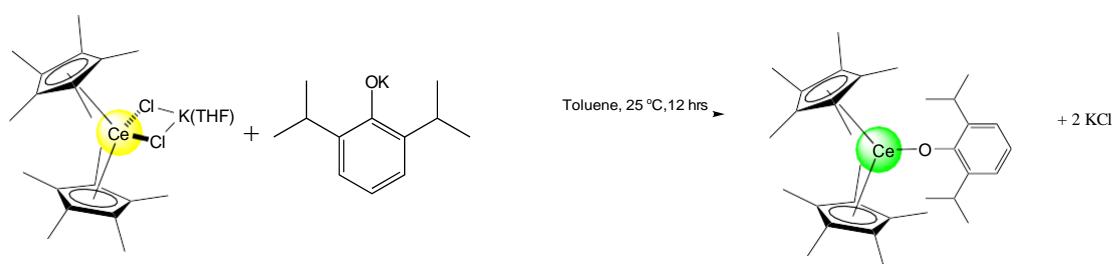
SCHEME 2.1: Reaction scheme presenting the synthesis of the cerium (III) aryloxide.

Cp*$_2$CeCl$_2$K (500 mg, 0.845 mmol) was dissolved in toluene (10 mL) and added to a 100 mL round bottom Schlenk flask. 10mL of KO-2,6-iPr$_2$C$_6$H$_5$ (182 mg, 0.845 mmol) in toluene was added dropwise. A color change occurred after 1 hour of stirring where solution turned from bright yellow to dark green. After continuous stirring at room temperature for 4 hours, the solvent then passed through a course frit into a 125 mL

filter flask to filter off KCl. The solvent was then removed via vacuo and extracted in pentane and filtered again through a celite pipette. The solution was then concentrated, and green crystals were obtained after cooling in pentane overnight at -20 °C. The ^{1}H and ^{13}C NMR spectra were taken in C_6D_6. Total yield: 0.2233 mg (0.329 mmol, 45%). 1H-NMR (600 MHz, benzene-d6): 9.14 (d, 2H, Ar-H), 8.60 (s, 1H, Ar-H), 3.03 (s, 30H, Cp*), -1.92 (s, 14H, , Ar-iPr), -4.53 (s, 4H), -6.53 (s, 2H,), -11.82 (m, 4H, Cp*). ^{13}C{^{1}H} NMR (600 MHz, C_6D_6) 126.48 (d, Ar-H), 120.74 (t, Ar-H) 40.1(s), 21.1(s, iPr), 20.9(s) , 15.55 (s), 6.6 (s, Cp*). 40, 21.0, 15.5. IR (cm^{-1}) 2953 (m), 2895 (m), 2857 (m), 1590 (s), 1432 (m), 1378 (s), 1324 (m), 1259 (m), 1201 (m), 1103 (s), 1019 (s), 849 (m), 747 (m), 649 (m), 561 (m). Elemental analysis calculated for $C_{32}H_{47}CeO$: (586.84 g/mol): C, 65.05%; H 8.109%. Found: C, 65.38%; H, 8.06%.
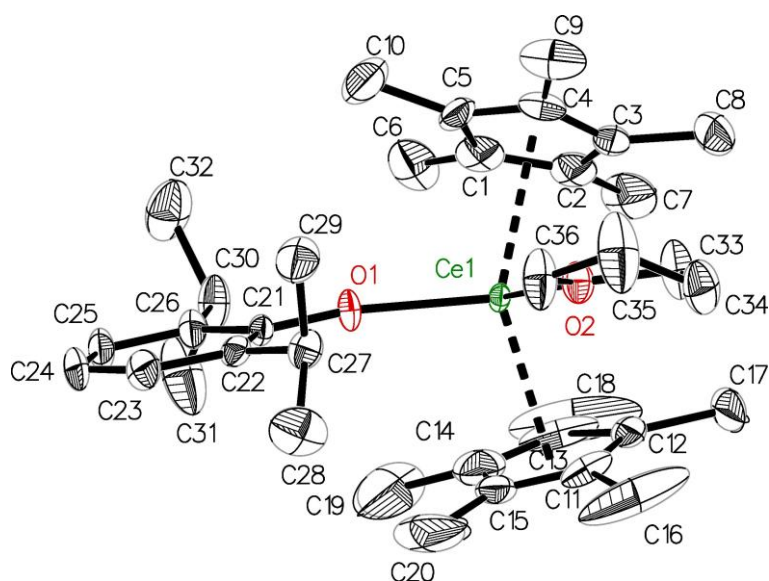
FIGURE 2.1: Thermal ellipsoid plot of Cp*$_2$Ce(O-2,6-iPr$_2$C$_6$H$_3$).

2.2.2 Synthesis of Cp*$_2$Ce(N(C$_6$H$_5$)$_2$)
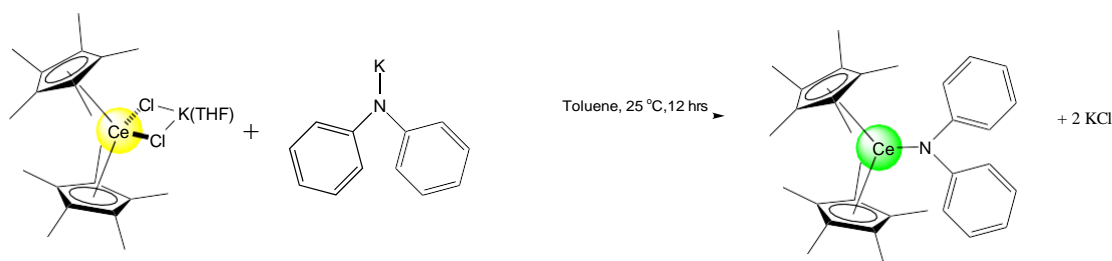
SCHEME 2.2: Reaction scheme involving the synthesis for the cerium (III) bisphenyl compound.

Cp*$_2$CeCl$_2$K (284.8 mg, 0.548mmol) was dissolved in THF (10 mL) and then 10 mL potassium bisphenyl amide in THF (10 mL) (113.6 mg, 0.548 mmol) is slowly added. The solution stays yellow and is allowed to stir at room temperature for 12 hours. The solvent is then pumped down to dryness to yield a yellow solid and then the product is extracted in 20 mL of pentane to yield a green solution. The green solution is then filtered through a celite pipette and pumped down to dryness. X-ray quality crystals are grown from slow vapor evaporation at -20 °C in pentane. ^{1}H-NMR (500 MHz, benzene-d6): δ 7.112 (t, 2H, Ar-H), 6.88(d, 2H, Ar-H), 6.82(t, 1H, Ar-H), 3.30 (br s, 30H Cp*),1.945 (s, 2H, Ar-H) -0.799(s, 5H, Ar-H), -16.98 (br s, 3H) 13C {1H} NMR (600 MHz, C$_6$D$_6$):δ 129.27 (t, Ar-H), 120.78(t, Ar-H), 120.05(s, Ar-H), 117.77(d, Ar-H), 112.4 (s, Ar-H), 10.3 (br, s) IR cm^{-1}: 2964 (m), 2899 (m), 2853 (m), 1578 (m), 1480(m), 1329 (m), 1204 (s), 1171 (s), 831 (s), 746 (m), 640(m), 516(m). Elemental analysis calculated for C$_{32}$H$_{40}$CeN: (578.43 g/mol): C, 66.41%; H 6.97% 2.42%. Found: C, 66.93%; H, 7.369%, 2.781%.
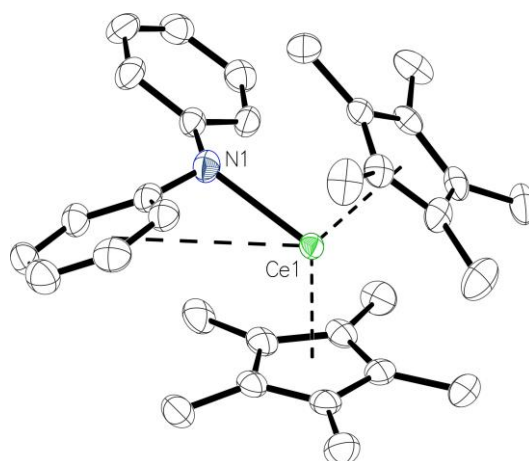
FIGURE 2.2: Thermal ellipsoid plot of Cp*$_2$Ce(N(C$_6$H$_5$)$_2$) shown at the 50% probability level. Hydrogen atoms associated with (C$_5$Me$_5$)$^{1-}$ ligands have been omitted for clarity. Ce-N bond length: 2.399 Å .

2.3 Results and Discussion

The reaction of (C$_5$Me$_5$)$_2$CeCl$_2$K(THF) with KO-2,6,^{i}Pr$_2$C$_6$H$_3$ and potassium diphenylamine, each resulted in a green crystalline solid as Cp*$_2$Ce(O-2,6-iPr$_2$C$_6$H$_3$ and a red crystalline solid as Cp*$_2$CeN(C$_6$H$_5$)$_2$. The solid state structures were determine by X-ray crystallography. Cp*$_2$Ce(O-2,6-iPr$_2$C$_6$H$_3$) demonstrated a pseudo-tetrahedral geometry around the metal center that contained two Ce-(C$_5$Me$_5$) centroids, the aryloxide O-2,6-iPr$_2$C$_6$H$_3$, and one THF solvent molecule. The Ce-O bond between the metal center and the aryloxide is 2.233 Å . The amide also contains a pseudo-tetrahedral geometry

however, the 4th bond is more of potential agostic integration with the phenyl group located on the amide. The Ce-N bond distance is 2.399 Å. The ^{1}H NMR demonstrates the Cp* peaks for the aryloxide and amide can be found at 3.03 and 3.25 ppm respectively.

In examining the photophysics of the Ce (III) compounds, one would expect that the different chemical environments around these two molecules would create different fluorescence spectra. However, fluorescence studies that utilized the absorbance values of each of the compounds demonstrate identical fluorescence patters. Figure 2.3 demonstrates the absorbance spectra for $Cp^*_2Ce(O\text{-}2,6\text{-}iPr_2C_6H_3)$, $Cp^*_2CeN(C_6H_5)_2$ and $Cp^*_2CeN(SiMe_3)_2$, which is already reported. [49] $Cp^*_2Ce(O\text{-}2,6\text{-}^iPr_2C_6H_3)$ contains absorbances at 375 nm ($\epsilon = 840$ L mol^{-1} cm^{-1}) with a slight shoulder at 435 nm ($\epsilon = 350$L mol^{-1} cm^{-1}) and a broad peak at 626 nm ($\epsilon = 350$ L mol^{-1} cm^{-1}). The doublet is present as a result of the transitions from the lowest 5d excited state to the spin-orbit split 4f ground state which is further split by spin-orbit interaction into two sublevels ($^2F_{5/2}$ and$^2F_{7/2}$). The amide has absorbance peaks at 435 nm ($\epsilon = 180$ L mol^{-1} cm^{-1}) and 522 nm ($\epsilon = 240$ L mol^{-1} cm^{-1}) These peaks are consistent with those found within the literature. [50–53] With regards to the bisphenyl amide, the compound is found to have absorbance at 417 nm ($\epsilon = 1800$) and 622 nm ($\epsilon = 350$ L mol^{-1} cm^{-1}).In utilizing these absorbance values, these compounds were excited at their respective absorbance wavelengths and the fluorescence data is demonstrated in Figure 2.4. For $Cp^*_2Ce(O\text{-}2,6\text{-}^iPr_2C_6H_3$ (a green colored solution), the compound absorbs both violet and orange light but emits only red light at 708 nm. For $Cp^*_2CeN(SiMe_3)_2$ (a red colored solu- tion), the compound absorbs indigo and green light while emitting orange light at 628 nm.Finally, the $Cp^*_2CeN(C_6H_5)_2$, the compound absorbs violet and orange light while its fluorescence pattern matches that of the aryloxide by fluorescing red light at 708 nm.
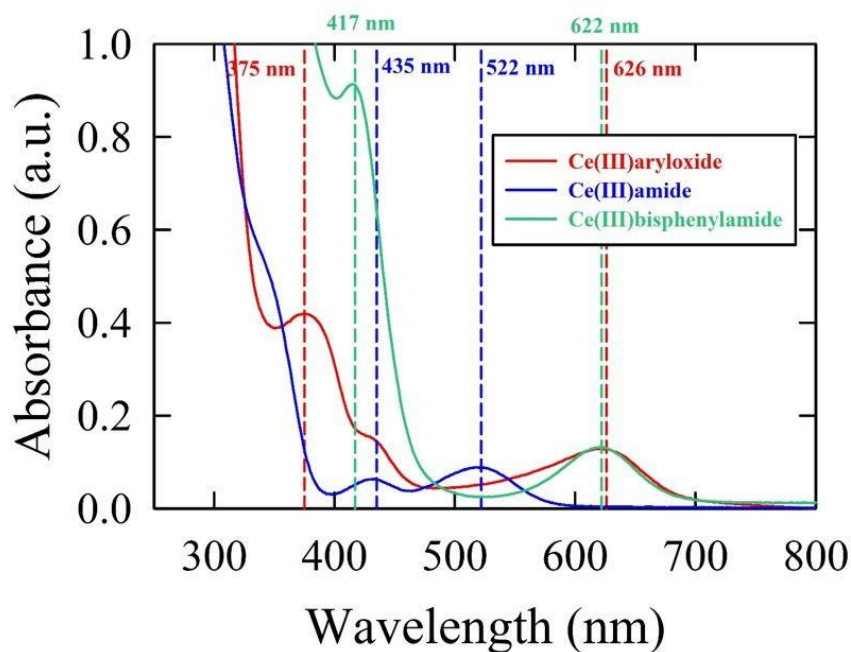
FIGURE 2.3: Variation of absorbance with wavelength for 0.5 mM Ce(III)aryloxide, Ce(III)amide, and Ce(III)bisphenylamide in pentane measured using a 1-cm path length cuvette. Sample was blank subtracted using a pentane solvent blank.
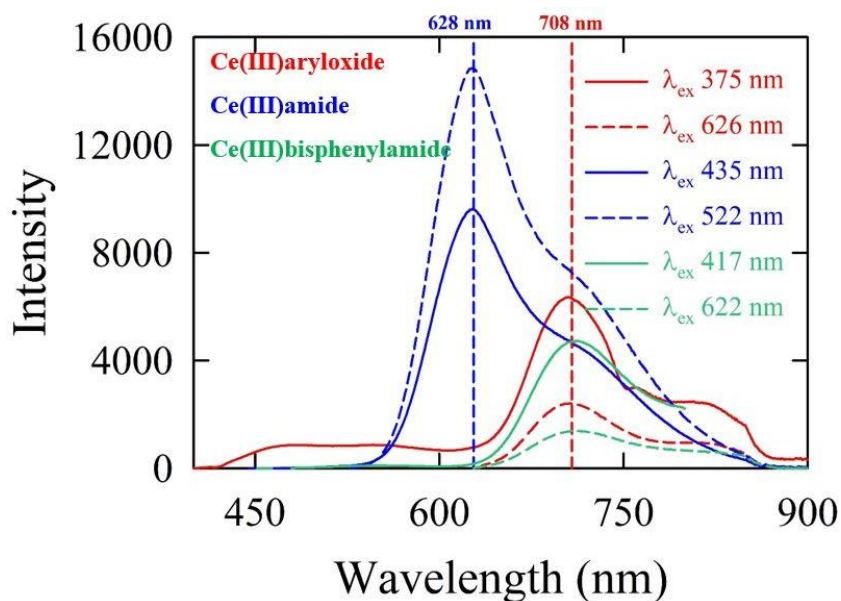
FIGURE 2.4: Variation of fluorescence intensity with wavelength for 0.5 mM Ce(III)aryloxide, Ce(III)amide, and Ce(III)bisphenylamide in pentane measured using a 1-cm path length cuvette (Excitation and emission band widths – 5.0 nm). Sample was excited at 375 nm, and 626 nm for Ce(III)aryloxide, 435 nm, and 522 nm for Ce(III)amide, and 417 nm and 622 nm for Ce(III)bisphenylamide (excitation wavelength obtained from UV-vis profile) and emission was scanned from 380900 nm, and 631900 nm for Ce(III)aryloxide, 440900 nm, and 527900 nm for Ce(III)amide , and 422800 nm, and 627900 nm for Ce(III)bisphenylamide respectively. Emissienviornmetson maximum was obtained at 628 nm for Ce(III)amide and at 708 nm for Ce(III)aryloxide and Ce(III)bisphenylamide.

2.4 Conclusion and Future Work

Within the data presented in this chapter, the similar fluorescence patters regarding both the aryl oxide and bisphenyl amide demonstrate that the two compounds share similar electronic structures despite their different atomic environments. Expansion on the investigation of Ce(III) complexes in varying environments can be continued in several ways. First, attempts should be made to alter the heteroatom attached to the aryl group. Utilizing group 15 and group elements will generate new atomic environments to explore and provide data specific to a new library of compounds. Current literature with Sm demonstrates the synthesis for $Cp^*_2SmE(C_6H_5)_2$ (E = P, As) which provides a foundation for the synthesis of analogous compounds with different lanthanides. [54]. If a similar synthetic approach is made for Ce, the fluorescence spectra for Ce-E (E = P,As) can be further explored.

Additionally, since the luminescence is affected by sterics, increasing the steric environment around the Ln(III) series by altering the alkyl groups on the aromatic ring may also generate new fluorescence data. As will be discussed in chapter 4, exploring the fluorescence of sterically encumbered terphenyl based ligands within the Ce(III) environment is worthwhile as the ligand and the metal are known to generate interesting photochemistry.

Chapter 3

Synthesis, Structure and Characterization of $Cp^*_2Ce^{IV}(O\text{-}2,6\text{-}iPr_2C_6H_3)$ X (X=I, Br, Cl, F) compounds.

3.1 Introduction

Cerium has attracted a large amount of attention in the recent years with Cyclopentadienyl ligands (Cp) are a staple in organo-lanthanide chemistry, including complexes involving the use of cerium. [55,56] The fist ever Ce(III) complex that utilized the Cp ligand was Cp_3Ce (C = C_5H_5). [57] Further utilization of the ligand brought about the isolation of cerium(III) ate complexes that contained mixtures of Cp*/halogenido moieties such as $Cp^*_2CeCl_2$K-(THF)$_2$, [$Cp^*_2CeI_2$] [K(THF)$_2$], as well as the half sandwich compound Cp^*CeI_2(THF). [52,53,58] While the cerium (III) complexes have gained a large amount of attention over the years, Ce(IV) complexes are quite rare. In synthesizing Ce(IV) compounds, choosing the proper ligand framework is crucial, particularly when it comes to oxidizing Ce(III) to Ce(IV). With recent work from the Walensky group focused on uranium heteroleptic metallocenes, such as $(C_5Me_5)U(OAr)$; (Ar = 2,4,6-Me$_3$C$_6$H$_2$, 4-^{t}BuC$_6$H$_4$ and 2,6-^{t}Bu$_2$-4-MeC$_6$H$_2$) [59] efforts were focused on synthesizing Ce(IV) compounds. Here we present a series of newly discovered Ce(IV) compounds that contain Cp*/halogen moieties.

3.2 Materials and Methods

All syntheses were carried out under an N_2 atmosphere using glovebox and Schlenk techniques unless otherwise stated. All non-deuterated solvents used were dried by passing through a solvent purification system (MBraun, USA) and stored over sieves, and potassium metal for aromatic and aliphatic solvents or calcium hydride for ethereal solvents.Cp*K[47], Cp*$_2$CeCl$_2$K[48], and Cp*$_2$CeN(SiMe$_3$)$_2$ [49], was prepared accordingly to their literature procedures. Benzene-d6 (Cambridge Isotope Laboratories) was degassed by three freezepumpthaw cycles and stored over molecular sieves. All ^{1} H spectra were taken on 600 MHz or 300 MHz Bruker spectrometers. All NMR chemical shifts are reported in ppm. ^{1}H NMR chemical shifts were referenced internally to the residual solvent peaks. IR spectra were recorded on a Nicolet Summit Pro FTIR spectrometer using a KBr pellet. Electronic absorption measurements were recorded in a sealed 1 cm quartz cuvette with a Varian Cary 5000 UVvisNIR spectrophotometer. Elemental analysis was performed on a Carlo Erba 1108 elemental analyzer, outfitted with an A/D converter for analysis using Eager Xperience software. SCXRD data was measured on a Bruker SMART diffractometer with an Apex II area detector (Bruker AXS LLC, USA) using Mo K radiation from a sealed source with focusing optics or on a Bruker D8 Venture with a Photon 100 CMOS area detector (Bruker AXS) using Mo K radiation from a microfocus source. Collection temperatures were controlled using Cryostream 700 and 800 cryostats (Oxford Cryosystems, UK). Hemispheres of data were collected using strategies of scans about the omega and phi axes. The Bruker Apex3 software suite was used for unit cell determination, data collection, and data reduction.

3.2.1 Experimental for Cp*$_2$Ce(O-2,6-iPr$_2$C$_6$H$_3$)(I)
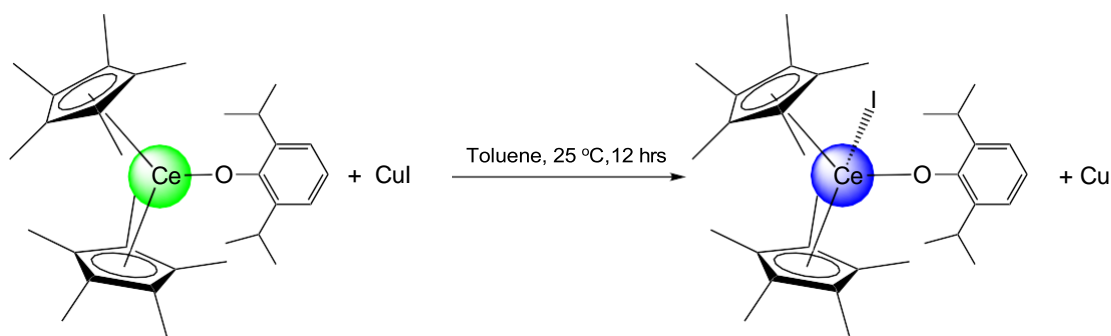
SCHEME 3.1: Reaction scheme for synthesis of the Ce(IV) iodide species. Synthesis involves reactuon with cerium (III) aryloxide and copper(I) iodide.

Cp*$_2$ Ce(O-2,6-iPr$_2$C$_6$H$_3$) (100mg, 0.148mmol) was dissolved in toluene (10 mL), and 5mL of CuI (28.1mg, 0.148 mmol) in toluene was added in to yield an initial green solution that then turned dark blue after stirring. After stirring at room temperature

for 15 min, the solvent was removed in vacuo then extracted in n-pentane and filtered through a celite containing pipette. Concentration of the filtrate yield crystals of Cp^*_2 $CeI(O-2,6-iPr_2C_6H_3)$ in quantitative yield. X-ray quality crystals were obtained from a concentrated n-pentane solution at -25 °C. The ^1H and ^{13}C NMR spectra were taken in C_6D_6. Total yield: 62 mg (0.0774 mmol, 62%). ^1H-NMR (500 MHz, benzene-d6): 7.42 (d, 2H, Ar-H), 6.35 (t, 1H, Ar-H), 5.39 (br s, 1H, iPr-H), 5.05 (br s, 1H, iPr-H), 4.33 (s, 29 H, Cp*), 3.92 (s, 1H, Cp*), 1.68 (s, 12 H, iPr-CH_3). IR (cm^{-1}): 2959 (s), 2904(s), 2865(s), 1432(s), 1423(m), 1378 (m), 1319(s), 1240(s), 1193(m), 1105 (s), 1092(s), 1014(s), 1020 (s), 885 (s), 850 (m), 793 (s), 754 (m), 689 (s), 570 (s)
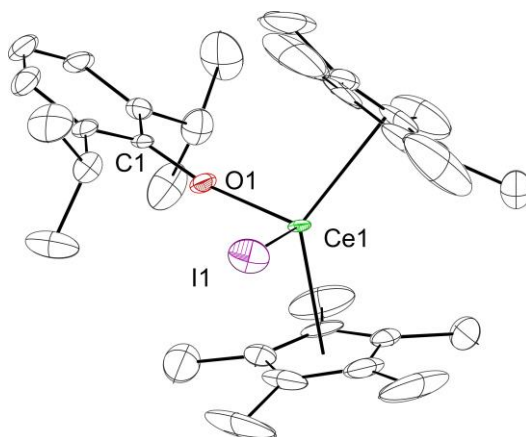
FIGURE 3.1: Thermal ellipsoid plot of $Cp^*2Ce(O-2,6-iPr_2C_6H_3)(I)$ shown at the 50% probability level. Hydrogen atoms associated with $(C_5Me_5)^{1-}$ ligands have been omitted for clarity.

3.2.2   Experimental for $Cp^*_2Ce(O-2,6-iPr_2C_6H_3)(Br)$
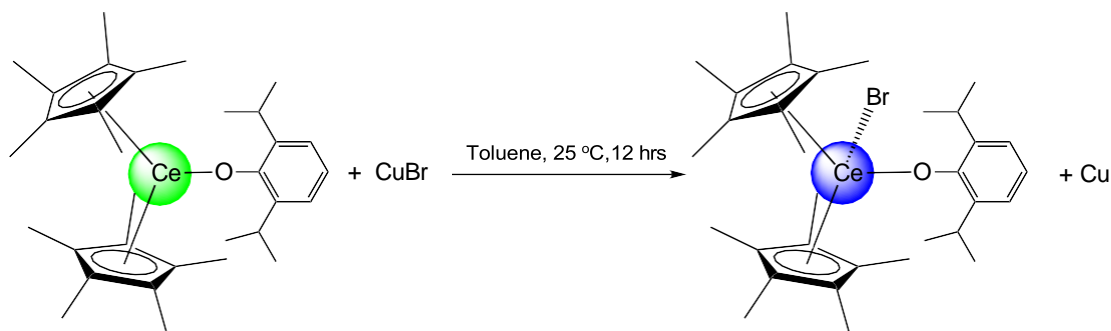
SCHEME 3.2: Reaction scheme for synthesis of the Ce(IV) bromide species. Synthesis involves reaction with cerium (III) aryloxide and copper(I) bromide

$Cp^*_2Ce(O-2,6-^iPr_2C_6H_5)$ (100 mg, 0.148 mmol) was dissolved in toluene (10 mL), and 5mL of CuBr (28.1mg, 0.148 mmol) in toluene was added in to yield an initial green

solution that then turned dark blue after stirring. After stirring at room tempera- ture overnight, the solvent was removed in vacuo then extracted in n-pentane and fil- tered through a celite containing pipette. Concentration of the filtrate yield crystals of $Cp^*_2CeBr(O-2,6-^iPr_2C_6H_5)$ in quantitative yield. X-ray quality crystals were ob- tained from a concentrated n-pentane solution at -25 °C. The ^1H and ^{13}C NMR spectra were taken in C_6D_6. ^1H-NMR (500 MHz, benzene-d6): 7.38 (dd, 2H, Ar-H), 7.01 (s, 1H, Ar-H), 5.16 (m, 1H, iPr-H), 4.99 (m, 1H, iPr-H), 4.00 (s, 30H, Cp*), 1.67 (dd, 12 H, iPr-CH3). ^{13}C {^1H} NMR (600 MHz, C_6D_6) 122.05 (t, Ar-H), 121.4(dd, Ar-H), 26.69(dd, iPr), 25.16 (dd, iPr), 10.75 (dd, iPr) 9.95 (s, Cp*). IR(cm-1) 2959 (m), 2914(m), 2861(m), 1654 (s), 1586 (s), 1429 (m), 1380 (m), 1320 (m), 1248 (m), 1194 (m), 1091 (s), 1061 (s), 886 (s), 855(m), 793 (s), 753 (m), 693(s), 624(s), 571(m). Elemental analysis calculated for $C_{32}H_{47}BrCeO$ (667.696 g/mol): C, 57.56%; H, 7.09%. Found: C, 57.28%; H. 6.686%.
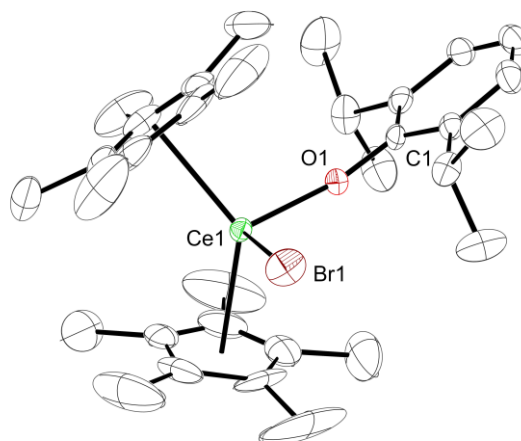
FIGURE 3.2: Thermal ellipsoid plot of $Cp^*_2Ce(O-2,6-iPr_2C_6H_3)(Br)$ shown at the50% probability level. Hydrogen atoms associated with $(C_5Me_5)^{1-}$ ligands have been omitted for clarity.

3.2.3   Experimental for $Cp^*_2Ce(O-2,6-iPr_2C_6H_3)(F)$
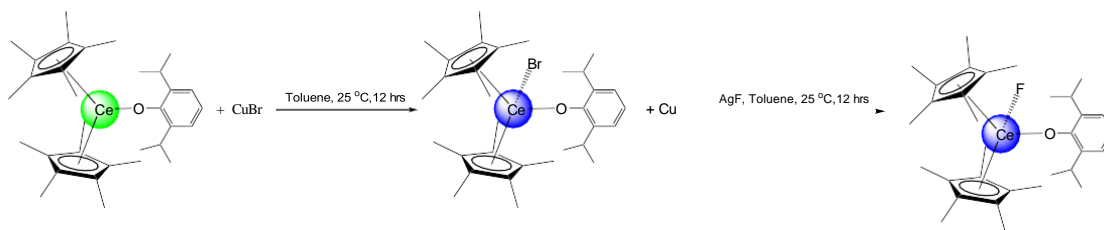
SCHEME 3.3: Two step synthesis for the creation of a Ce(IV)-F compound. First step involves synthesis of the bromide which is then further reacted with AgF to create the fluoride and filter off Ag metal.

Cp*$_2$CeBr(O-2,6-iPr$_2$C$_2$H$_5$) (15.3 mg, 0.022 mmol) was dissolved in toluene (10 mL) and then AgF in toluene (10 mL) (2.9 mg, 0.022 mmol) is slowly added. The solution remains dark blue and is allowed to stir at room temperature overnight. The solvent is then pumped down to dryness to yield a dark blue solid and then extracted in 20 mL of pentane. The pentane solution is filtered through celite and concentrated. ^{1}H- NMR (500 MHz, benzene-d6): 7.09 (d, 2H, Ar-H), 6.61 (t, 1H, Ar-H), 5.16 (m, 1H, iPr-H), 5.00(m iPr-H) 4.10 (s, 30H, Cp*), 1.67 (dd, 12H, iPr-CH$_3$) $_{13}$C NMR (600 MHz, C$_6$D$_6$): 122.39(d, Ar-H), 121.32(t, Ar-H), 27.16(m ipr-H), 25.17(m, ipr-H), 10.13(s, Cp*, 9.94(dd, 12H, iPr-CH$_3$). ^{19}F (600 MHz, C$_6$D$_6$): 332.69 (s, Ce-F)

3.3 Discussion

Treatment of Cp*$_2$CeCl$_2$K with KO-2,6-iPr$_2$C$_2$H$_5$ in toluene yields the Ce(III) compound Cp*$_2$Ce(O-2,6-iPr$_2$C$_6$H$_3$)as a green crystal in 45% yield.With the recently reported Ce(IV) compound Cp*$_2$CeCl(O-2,6-iPr$_2$C$_6$H$_3$) isolated and published by Anwander, initial attempts were made to develop an alternative synthetic route. Further treatment of this compound with one electron oxidants such as CuX (X = I,Br,Cl) provide the respective Ce(IV) halide compound. While each reaction lead to a color change of green to dark blue and treatment of Cp*$_2$Ce(O-2,6-iPr$_2$C$_6$H$_3$) with CuBr and CuI cleanly provide Cp*$_2$CeI(O-2,6-iPr$_2$C$_6$H$_3$) and Cp*$_2$CeBr(O-2,6-iPr$_2$C$_6$H$_3$), attempts to isolate Cp*$_2$CeF(O-2,6-iPr$_2$C$_6$H$_3$) have been difficult.

To obtain Cp*$_2$CeF(O-2,6-iPr$_2$C$_6$H$_3$) several fluorinating agents were used. It is worth noting that while fluoride salts of varying degree have been utilized to oxidize U(III) to U(IV), Ce(III) is less reducing than U(III) thus requiring less potent oxidizing agents. As a result of this, initial attempts focused on utilizing copper and silver fluoride salts. Even though a blue color change did occur in both instances, the ^{1}H NMR did not contain proton peaks for C$_5$H$_5$. Additionally, ^{19}F NMR for both cases provided peaks at around 14 ppm which do not match with the reported ^{19}F peak from CeF(N(SiMe)$_2$)$_3$ at +319 ppm. Given Schelters success with ferrocinium salts, ferrocinium hexafluorophosphate was reacted with Cp*$_2$Ce(O-2,6-iPr$_2$C$_6$H$_3$) and produced a Ce-F complex's that contained ^{1}H and ^{19}F which contained the proper peaks, specifically the ^{19}F peak at 307ppm. Obtaining a crystal of the complex was difficult as crystallization would compete with ferrocene. To eliminate this, more successful attempts were made through a successive salt metathesis route displayed in Scheme A.2. Treatment of Cp*$_2$Ce(O- 2,6-iPr$_2$C$_6$H$_3$) with CuBr produces Cp*$_2$CeBr(O-2,6-iPr$_2$C$_6$H$_3$) which can be further reacted with AgF to cleanly produce Cp*$_2$CeF(O-2,6-iPr$_2$C$_6$H$_3$).

In examining the isolated structures of $Cp^*_2CeBr(O-2,6-iPr_2C_6H_3)$ and $Cp^*_2CeI(O-2,6-iPr_2C_6H_3)$, the ^{1}H NMR spectra demonstrates a correlation between the $(C_5Me_5)^{-1}$ resonance specifically referring to the π-donation from the halide and is demonstrate in

The solid-state structure of $Cp^*_2CeBr(O-2,6-iPr_2C_6H_3)$ and $Cp^*_2CeI(O-2,6-iPr_2C_6H_3)$ were determined by X-ray crystallographic analysis. Each complex contains a short Ce-O bond distance of 2.133(2) and 2.135(4) respectively, which is similar to the 2.150(10) in $Cp^*_2CeCl(O-2,6-iPr_2C_6H_3)$ as well as the 2.151(4) in $[(C_5H_5)_3Ce(O-2,6-{}^iPr_2C_6H_3)]$, 2.113(2)-2.145(2) in $Ce(MBP)_2(THF)_2$, MBP = 2,2-methylenebis(6-tert-butyl-4-methylphenolate), and 2.194(2)-2.221(2) in $Ce(ArOSeO)_2(bipy)$, ArOSeO = 2,2-selenobis(4,6-di-tert-butylphenolate.[60] The Ce-Br and Ce-I bond distances of 2.8109(5) and 3.0715(6), respectively, are longer than those in $[CeN(SiMe_3)_2)_3)X]$ complexes of 2.766(2), X = Br, and 2.9980(2), X = I.[61] The widening of the X-Ce-O bond angle is observed moving from 104.5(3) to 105.68(11) as the halide becomes larger.

TABLE 3.1: Selected bond distances (Å) and angles (deg) as well as $(C_5Me_5)^{1-}$) resonance in ^{1}H NMR (ppm) is tabulated. Data for chloride providied by Anwander[16]

Compound	Ce-O (Å)	Ce-X (Å)	Ce-O-C$_{ipso}$(deg)	$(C_5Me_5)^{1-}$) resonance (ppm)
X = THF				3.03
X = Cl[16]	2.150(10)	2.638(5)	162.1(9)	3.93
X = Br	2.133(2)	2.8109(5)	163.2(2)	4.10
X=I	2.135(4)	3.0715(6)	163.9(4)	4.33

3.4 Future Work

Future investigations into exploring the structure and reactivity of these types of elements can occur in several ways. Since fluoride compounds are rare, further investigation into other reagents would be extremely beneficial as they may provide cleaner and more efficent synthetic routes Reagents such as trityl hexafluorophosphate, or derivatives of ammonium hexafluorostannate should be investigated. In doing this, one can potentially optimize the reaction conditions and explore new ways to generate fluorine delivering agents.

Additionally, this same project should be investigated with the use of a bisphenyl amide or bisphenyl phosphine. Focusing on different ligands will alter the chemical environment around the lanthanide metal center and new reactivity can be explored.

Chapter 4

Synthesis Structure of β diketones

4.1　Introduction

With the staple β diketone ligands such as benzoylacetone (bzac), acetylacetonate (acac), and dibenzoylmethane (dbm) setting the stage for various β diketone complexes to be discovered, realization of their potential grew rapidly. As the rich coordination chemistry of these molecules was explored, it was discovered that applications are useful for single molecule magnets, luminescence, molecular sensing, heavy metal waste treatment, and various forms of biochemistry. As mentioned earlier, most diketones contained alkyl or phenyl substituents however, exploration of sterically hindered diketones took off in 1960. Within this chapter we present several new cerium based compounds that contain β diketones, as well as their synthetic method, NMR and crystal structure.

4.2　Materials and Methods

All syntheses were carried out under an N_2 atmosphere using glovebox and Schlenk techniques unless otherwise stated. All non-deuterated solvents used were dried by passing through a solvent purification system (MBraun, USA) and stored over sieves, and potassium metal for aromatic and aliphatic solvents or calcium hydride for ethereal solvents. The H(Mes-Ph$_6$) and H(esac) ligands were provided by Marshak's group at University of Colorado Boulder and used as is. Benzene-d6 (Cambridge Isotope Laboratories) was degassed by three freezepumpthaw cycles and stored over molecular sieves. All [1] H spectra were taken on 600 MHz or 300 MHz Bruker spectrometers. All NMR chemical shifts are reported in ppm. ^{1}H NMR chemical shifts were referenced internally to the residual solvent peaks. IR spectra were recorded on a Nicolet Summit Pro FTIR spectrometer using a KBr pellet. Electronic absorption measurements were recorded in a sealed 1

cm quartz cuvette with a Varian Cary 5000 UVvisNIR spectrophotometer. Elemental analysis was performed on a Carlo Erba 1108 elemental analyzer, outfitted with an A/D converter for analysis using Eager Xperience software. SCXRD data was measured on a Bruker SMART diffractometer with an Apex II area detector (Bruker AXS LLC, USA) using Mo K radiation from a sealed source with focusing optics. All crystal structures were collected on a Bruker D8 Venture with a Photon 100 CMOS area detector (Bruker AXS) using Mo K radiation from a microfocus source. Collection temperatures were controlled using Cryostream 700 and 800 cryostats (Oxford Cryosystems, UK). Hemispheres of data were collected using strategies of scans about the omega and phi axes. The Bruker Apex3 software suite was used for unit cell determination, data collection, and data reduction.

4.2.1 Experimental for K(Mes-Ph$_6$)
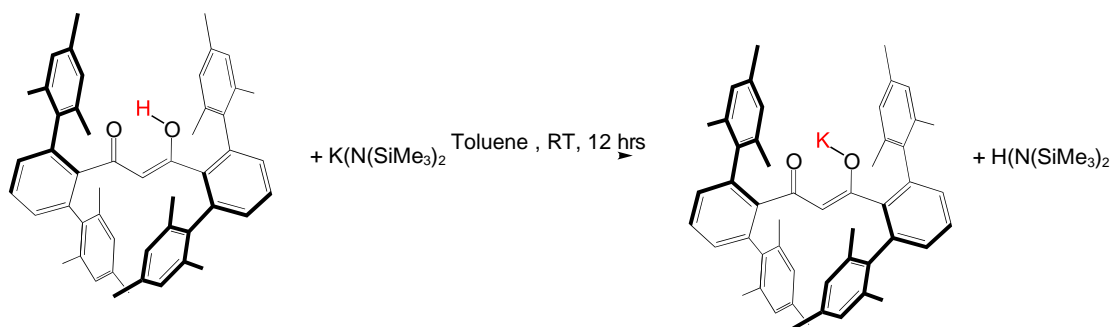
SCHEME 4.1: Reaction scheme for the potassiated Mes-Ph$_6$ through the use of a sterically hindered strong base.

KN(SiMe$_3$)$_2$ (12 mg , 0.060 mmol) was dissolved in toluene (10 mL), and 5mL of H(Mes-Ph$_6$) (27.2 mg, 0.039 mmol) in toluene was added in to yield an initial colorless solution that then turned light red stirring overnight. After stirring at room temperature overnight, the solvent was removed in vacuo then extracted in n-pentane and filtered through a celite containing pipette. Concentration of the filtrate yield crystals of K

(Mes-Ph$_6$). X-ray quality crystals were obtained from a concentrated n-pentane solution at -25 °C. The ^{1}H and ^{13}C NMR spectra were taken in C$_6$D$_6$. Total yield: 20 mg (0.0292 mmol, 50%). ^{1}H-NMR (500 MHz, benzene-d6): 16.84 (s, 1H), 7.01 (br s, 5H, Ar-H), 6.97 (s, 4H, Ar-H), 6.8 (s, 8H, Ar-H), 6.79 (d, 5H, Ar-H), 6.75(d,9H, Ar-H), 5.0 (s, 1H), 4.95 (s, 1H), 2.35 (s, 9H), 2.20 (s, 11H), 2.17 (s, 11H), 1.90 (s, 24H)
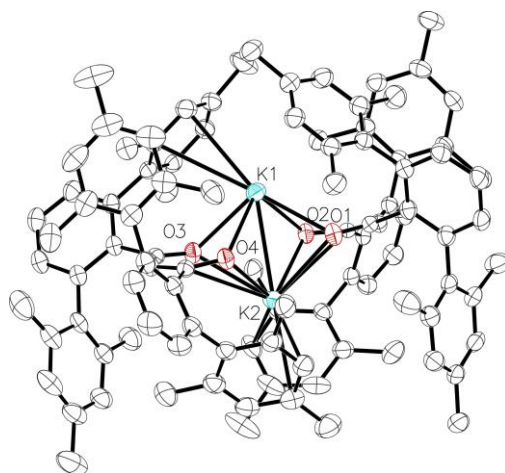
FIGURE 4.1: Thermal ellipsoid plot of K(Mes-Ph$_2$) shown at the 50% probability level.

4.2.2 Experimental for Ce(esac)((N(SiMe$_3$)$_2$)$_2$
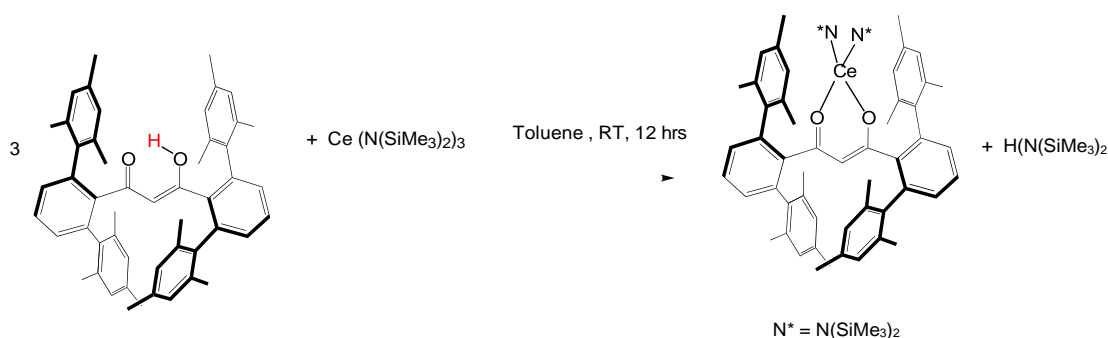
SCHEME 4.2: Reaction scheme of three equivalents of H(Mes-Ph$_6$) and Cerium(III) Tris(bis(trimethylsilyl)amide). The steric hindrance of the ligand prohibits the attachment of 3 ligands onto the metal center.

Ce(N(SiMe$_3$)$_2$)$_3$ (62 mg, 0.0997 mmol) was dissolved in toluene (10 mL), and 5 mL of H(Mes-Ph$_6$) (208 mg, 0.298 mmol) in toluene was added in to yield an initial colorless solution that then turned light red stirring overnight. After stirring at room temperature overnight, the solvent was removed in vacuo then extracted in n-pentane and filtered through a celite containing pipette. Concentration of the filtrate yield crystals of K(Mes-Ph$_6$) in quantitative yield. X-ray quality crystals were obtained from a concentrated n-pentane solution at -25 °C. The ^{1}H and ^{13}C NMR spectra were taken in C$_6$D$_6$. Total yield: 60 mg (0.0292 mmol, 90%). ^{1}H-NMR (500 MHz, benzene-d6): 17.42(br s, 1H), 8.04(s, 2H, Ar-H), 7.42(s, 4H, Ar-H), 6.81(s, 3H, Ar-H), 5.82(br s, 8H Ar-H) 2.66(br, s), 2.17 (s, 2H), 1.90 (s, 2H), 1.22(s, 11H), 0.88(s, 10H), 0.97(s, 2H), -2.0(br s, 11.1), -5.8(br s, 24H)
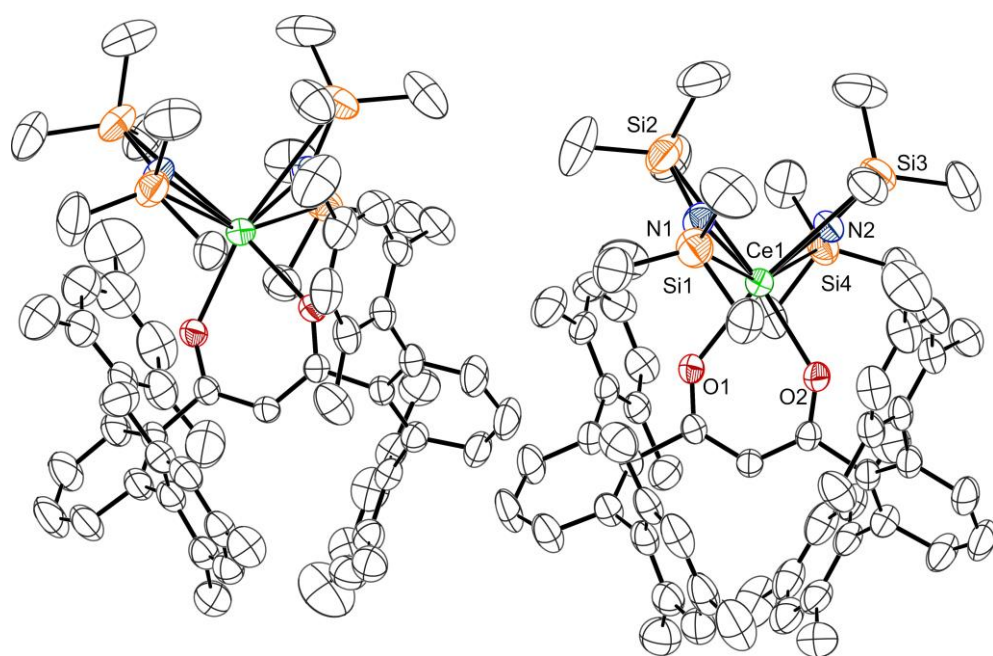
FIGURE 4.2: Thermal ellipsoid plot of Ce(Mes-Ph$_6$)N$^*_2$ shown at the50% probability level.

4.2.3 Experimental for Ce^{III}(esac)$_3$
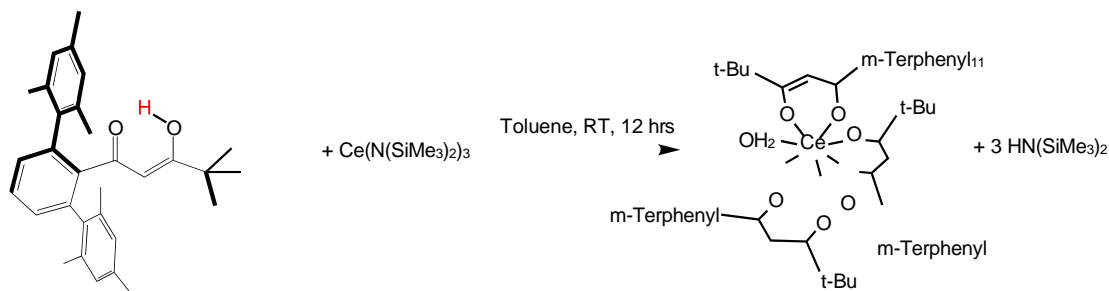
SCHEME 4.3: Reaction scheme for the synthesis of Ce^{III}(esac)$_3$ through the use of the H(esac) ligand.

Ce(N(SiMe$_3$)$_2$)$_3$ (76.9 mg, 0.123 mmol) was dissolved in toluene (10 mL), and 5mL of H(esac) (163.7 mg, 0.3715 mmol) in toluene was added in to yield an initial colorless solution that then turned light red stirring overnight. After stirring at room temperature overnight, the solvent was removed in vacuo then extracted in n-pentane and filtered through a celite containing pipette. Concentration of the filtrate yield crystals of Ce(esac)$_3$ in quantitative yield. X-ray quality crystals were obtained from a concentrated n-pentane solution at -25 ^{o}C. Total yield: 69.7mg (0.038 mmol, 90%).
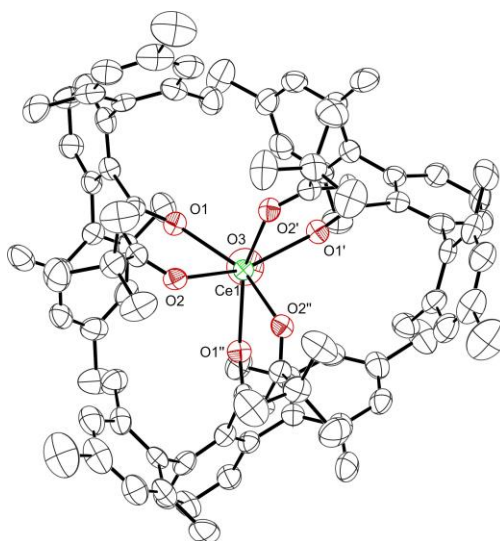
FIGURE 4.3: Thermal ellipsoid plot of Ce^{III}(esac)$_3$ shown at the50% probability level.

4.2.4 Experimental for Ce^{III}(Mes-Ph$_3$)$_2$
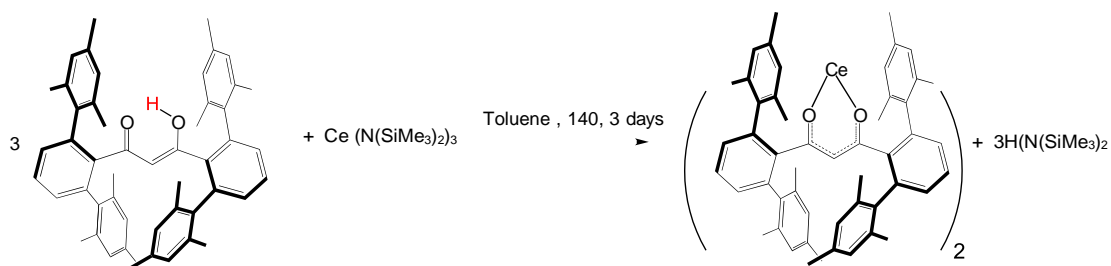
SCHEME 4.4: Reaction scheme for the synthesis of Ce(Mes-Ph$_6$)$_2$

Ce(N(SiMe$_3$)$_2$)$_3$ (66.4 mg, 0.106 mmol) was dissolved in toluene (10 mL), and 5mL of H(Mes-Ph$_6$) (223 mg, 0.320 mmol) in toluene was added in to yield an initial colorless solution that then turned light red stirring overnight. After stirring at 140 ^{o}C for three days, the solvent was removed in vacuo then extracted in n-pentane and filtered through a celite containing pipette. Concentration of the filtrate yield crystals of Ce(Mes-Ph$_6$)$_2$ in quantitative yield. X-ray quality crystals were obtained from a concentrated n-pentane solution at -25 ^{o}C. Total yield: 69.7mg (0.038 mmol, 90%).
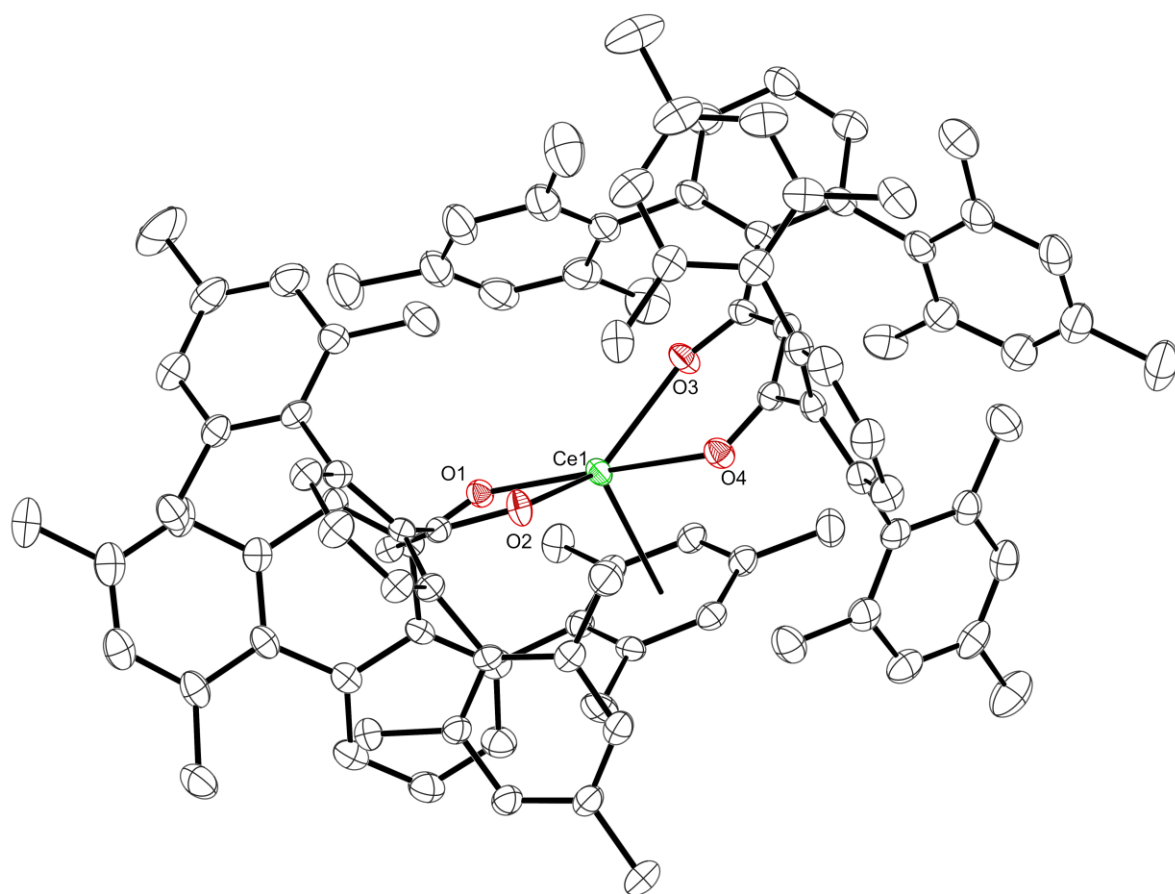
FIGURE 4.4: Thermal ellipsoid plot of $Ce^{III}(Mes-Ph_6)_2$

4.3 Discussion

Attempts at utilizing sterrically encumbered acac ligands focused on attaching three ligands around one cerium metal center. Treatment of $Ce(N(SiMe_3)_2)_3$ with H(esac) or $H(Mes-Ph_6)$ provided various cerium-β diketone compounds. Each solid state structure was determined by X-ray crystallography. Initial salt metathesis reactions with anhydrous $CeCl_3$ were unsuccessful, however isolation of the potassium salt was achieved and is depicted in Figure 4.1 . Upon reacting $H(Mes-Ph_6)$ with $K(N(SiMe_3)_2)$, the reaction turned from colorless to red. ^{1}H NMR depicts peaks for both the protonated and potassium salt as evident by the peaks at 2.35, 2.20, 2.17, and 1.90 ppm. Addition- ally, presence of the hydroxide peak at 5.10 indicates the presence of unreacted starting material. As a result of both compounds being soluble in pentane, both compounds crystallised together but were able to be distinguished by their color. The solid state structure of $K(Mes-Ph_6)$ exists as a red crystal whose potassium atoms adopt a dimeric form. This dimer contains a diamond core center where the K atom is coordinated to

36

both oxygen's in each of the Mes-Ph$_6$ ligand and has η^6 coordination to one phenyl ring in each respective Mes-Ph$_6$ ligand.

Additionally, treatment of Ce(N(SiMe$_3$)$_2$)$_3$ with three equivalents of H(Mes-Ph$_6$) resulted a yellow solution that turned red and produced the cerium complex depicted in Figure 4.2, where a single Mes-Ph$_6$ attached to the compound. ^{1}H NMR resulted in several broad peaks at 5.63, 2.66, -1.86, -5.69. Within this structure cerium is found to be in a tetrahedral geometry. Further reactions involving the same reagents and stoichiometry occurred in a pressure tube and heated to 140°C for three days. This resulted in a color change from yellow to red as well as trivalent cerium species that contained two Mes-Ph$_6$ ligands. To maintain the trivalent oxidation state, one Mes-Ph$_6$ ligand had to adopt a dianionic state to allow for two X-type interactions with the metal center. Additionally, upon examination of the solid state structure, all Ce-O bonds occur around the same plane which generates a single η^6 interaction, that exists alomost 90 ^{o}C to the Ce-O bonds, to a flanking phenyl ring providing a pesudo pentagonal pyramidal geometry around the metal center. Given that sterics play a significant role within these compounds, attention was then turned towards H(esac) as its [t]Bu group allows for more flexibility and less steric interactions than two terphenyl moieties.

Treatment of Ce(N(SiMe$_3$)$_2$)$_3$ with three equivalents of H(esac) provide a yellow solution that turned red and produced a Ce(III) complex as depicted in Figure 4.3. While the solid state structure does contain three esac ligands bound to the metal center, water contamination generated a aqua ion to bind to the metal center.

4.4   Future Work

Future work with this project should lead to the following: With Cp* ligands being a staple within organometallic chemistry, exploration with other ligand frameworks is necessary to generate new and interesting chemistry. Given that three esac ligands were able to bind to cerium, further studies should focus on utilizing this compound to explore Ce(III) and Ce(IV) reactivity. More specifically, this project is walking in the footsteps of the previous project involving the Cp$^*_2$Ce(O-2,6-iPr$_2$C$_6$H$_3$), framework. While the the presence of the aqua ion is not ideal, it demonstrates the the ligand framework is flexible enough to react with either small molecules (CO,CO$_2$, etc.), or one electron reactants (CuX, X = I, Br, Cl, F) and generate new Ce(IV) compounds.

Additionally, since Ce was utilized, further investigations should focus on other lanthanides such as lutetium to investigate if the ligand has the potential to attach to the entire lanthanide series. Additionally, since 2 Mes-Ph$_6$ ligands can react with the metal

center to form a dianionic species, reactions with divalent lanthanides should also be explored. If reactions prove successful, small molecule activation studies are worthwhile investigations. Additionally, given the ligands prestige within fluorescence chemistry and the unique η^6 interactions that stabilize the metal, further fluorescence studies should be performed to investigate how variations in sterics affects cerium fluorescence.

Appendix A

Additional Experimental and Crystal Structures

A.0.1   Experimental for Cp*$_2$ThCl(O-2,6-iPr$_2$C$_6$H$_3$)
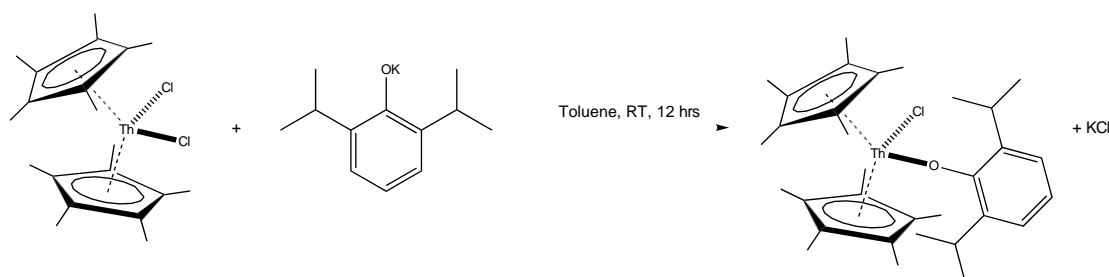
SCHEME A.1: Snythetic scheme for the synthesis of Cp*$_2$ThCl(O-2,6-iPr$_2$C$_6$H$_3$).

Cp*$_2$ThCl$_2$ (71 mg, 0.123 mmol) was dissolved in toluene (5mL) and 5 mL toluene solution of KO-2,6-iPr$_2$C$_6$H$_3$ was added. The reaction was allowed to stir overnight and remained colorless the entire time. After the reaction period, the solvent was removed via vacuo and the compound was extracted in pentane. The pentane solution was filtered through a celite containing pipette and then pumped down to dryness. Yield: 65 mg, 0.090 mmol (92%). ^{1}H NMR (600 MHz, C$_6$D$_6$): 7.11 (d, 2H, Ar-H), 6.92(t, 1H, Ar-H), 3.39 (m, 2H, ^{i}Pr-H), 2.01 (s, 30H, Cp*), 1.38(d, 12H, ^{i}Pr).
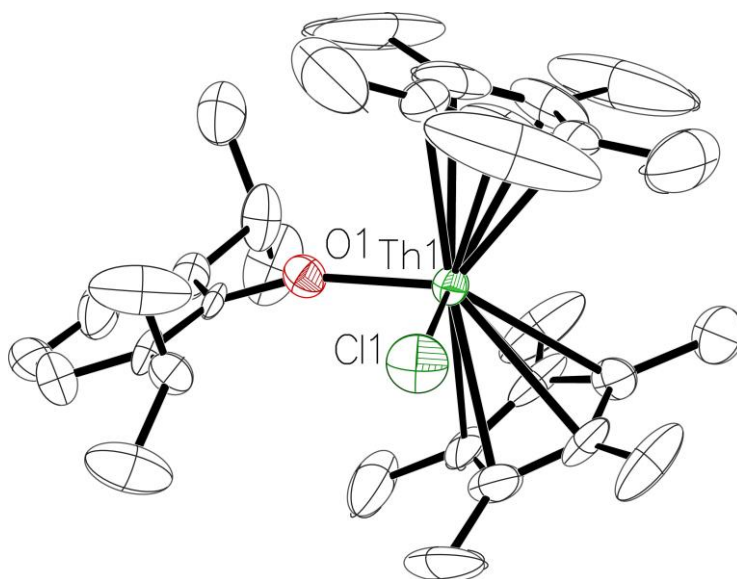
FIGURE A.1: Thermal ellipsoid plot of Cp*$_2$ThCl(O-2,6-iPr$_2$C$_6$H$_3$)

A.0.2 Experimental for Cp*$_2$ThCl(O-2,6-iPr$_2$C$_6$H$_3$)
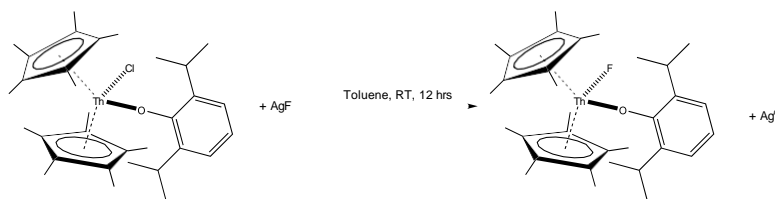
SCHEME A.2: Snythetic scheme for the synthesis of Cp*$_2$ThCl(O-2,6-iPr$_2$C$_6$H$_3$).

Cp*$_2$ThCl(O-2,6-iPr$_2$C$_6$H$_3$) (65 mg, 0.090 mmol) was dissolved in toluene (5mL) and excess AgF was added. The reaction was allowed to stir overnight and remained colorless the entire time. After the reaction period, the solvent was removed via vacuo and the compound was extracted in pentane. The pentane solution was filtered through a celite containing pipette and then pumped down to dryness. Yield: 60 mg, 0.085 mmol (92%). ^{1}H NMR: (600 MHz, C$_6$D$_6$): 7.11 (dd, 2H, Ar-H), 6.92(t, 1H, Ar-H), 3.39 (m, 2H, ^{i}Pr-H), 2.01 (s, 30H, Cp*), 1.38(d, 12H, ^{i}Pr). ^{13}C (600 MHz, C$_6$D$_6$): 123.8(dd, Ar-H), 120.75 (t, Ar-H), 26.86 (m,^{i}Pr-H), 24.3 (d, ^{i}Pr), 11.27 (s, Cp*). ^{19}F NMR (300 MHz, C$_6$D$_6$): 192.87.

Bibliography

[1] Barry Kilbourn. *Cerium and Cerium Compounds*, volume 5. 11 2003. ISBN 9780471238966. doi: 10.1002/0471238961.0305180911091202.a01.pub2.

[2] William J Evans. The importance of questioning scientific assumptions: some lessons from f element chemistry. *Inorganic chemistry*, 46(9):3435—3449, April 2007. ISSN 0020-1669. doi: 10.1021/ic062011k. URL https://doi.org/10.1021/ic062011k.

[3] Jean-Claude G. Bünzli. Lanthanide photonics: Shaping the nanoworld. *Trends in Chemistry*, 1(8):751–762, 2019. ISSN 2589-5974. doi: https://doi.org/10.1016/j.trechm.2019.05.012. URL https://www.sciencedirect.com/science/article/pii/S2589597419301406.

[4] Ukrae Cho and James K. Chen. Lanthanide-based optical probes of biological systems. *Cell chemical biology*, 27(8):921–936, 2020. ISSN 2451-9448 2451-9456. doi: 10.1016/j.chembiol.2020.07.009. URL https://pubmed.ncbi.nlm.nih.gov/32735780https://www.ncbi.nlm.nih.gov/pmc/articles/PMC7484113/. 32735780[pmid] PMC7484113[pmcid] S2451-9456(20)30282-8[PII].

[5] Owen Bailey, Samra Husremovic, Madison Murphy, Jason Ross, Joyce Gong, Daniel Olds, and Geneva Laurita. Compositional influence of local and long-range polarity in the frustrated pyrochlore system bi2xrexti2o7 (re = y3+,ho3+). *J. Mater. Chem. C*, pages –, 2022. doi: 10.1039/D2TC01328B. URL http://dx.doi.org/10.1039/D2TC01328B.

[6] Steven J. Gray, Karen Brown, Francis Y. T. Lam, Jennifer A. Garden, and Polly L. Arnold. Dinuclear ce(iv) aryloxides: Highly active catalysts for anhydride/epoxide ring-opening copolymerization. *Organometallics*, 40(7):948–958, 2021. ISSN 0276-7333. doi: 10.1021/acs.organomet.1c00055. URL https://doi.org/10.1021/acs.organomet.1c00055. doi: 10.1021/acs.organomet.1c00055.

[7] John Wiley and Sons. *Rare Earth Coordination Chemistry - Fundamentals and Applications*. 2010.

[8] V. V. Nikonorov. Determination of the stability constants of lanthanide complexes with oxyacids using capillary electrophoresis. *Journal of Analytical Chemistry*, 65 (4):359–365, 2010. ISSN 1608-3199. doi: 10.1134/S1061934810040040. URL https://doi.org/10.1134/S1061934810040040.

[9] Zuqiang Bian and Chunhui Huang. *Rare Earth Coordination Chemistry: Fundamentals and Applications*, pages 391 – 420. 01 2008. ISBN 9783527621309. doi: 10.1002/9783527621309.ch12.

[10] K. A. Gschneidner. On the nature of 4 bonding in the lanthanide elements and their compounds. *Journal of the Less Common Metals*, 25(4):405–422, 1971. ISSN 0022-5088. doi: https://doi.org/10.1016/0022-5088(71)90184-6. URL https://www.sciencedirect.com/science/article/pii/0022508871901846.

[11] Takanori Shima, Yi Luo, Timothy Stewart, Robert Bau, Garry J. McIntyre, Sax A. Mason, and Zhaomin Hou. Molecular heterometallic hydride clusters composed of rare-earth and d-transition metals. *Nature Chemistry*, 3(10):814–820, 2011. ISSN 1755-4349. doi: 10.1038/nchem.1147. URL https://doi.org/10.1038/nchem. 1147.

[12] L.J. Nugent, R.D. Baybarz, J.L. Burnett, and J.L. Ryan. Electron-transfer and f d absorption bands of some lanthanide and actinide complexes and the standard (iii–iv) oxidation potentials for each member of the lanthanide and actinide series. *Journal of Inorganic and Nuclear Chemistry*, 33(8):2503–2530, 1971. ISSN 0022-1902. doi: https://doi.org/10.1016/0022-1902(71)80226-9. URL https://www.sciencedirect.com/science/article/pii/0022190271802269.

[13] Zhifeng Zhang, Hongfei Li, Fuqiang Guo, Shulan Meng, and Deqian Li. Synergistic extraction and recovery of cerium(iv) and fluorin from sulfuric solutions with cyanex 923 and di-2-ethylhexyl phosphoric acid. *Separation and Purification Technology*, 63:348–352, 2008.

[14] Dongli Zhang, Wei Wang, Yuefeng Deng, Jianping Zhang, He Zhao, and Ji Chen. Extraction and recovery of cerium(iv) and fluorine(i) from sulfuric solutions using bifunctional ionic liquid extractants. *Chemical Engineering Journal*, 179:19–25, 2012.

[15] ZOU Dan, CHEN Ji, and LI Deqian. Separation chemistry and clean technique of cerium(iv): A review. *Journal of Rare Earths*, 32(8):681–685, 2014. ISSN 1002-0721. doi: https://doi.org/10.1016/S1002-0721(14)60125-3. URL https://www.sciencedirect.com/science/article/pii/S1002072114601253.

[16] Lars Hirneise, Cäcilia Maichle-Mössmer, and Reiner Anwander. Pentamethylcy-clopentadienyl complexes of cerium(iv): Synthesis, reactivity, and electrochemistry. *Inorganic Chemistry*, 60(23):18211–18224, 2021. ISSN 0020-1669. doi: 10.1021/acs. inorgchem.1c02851. URL https://doi.org/10.1021/acs.inorgchem.1c02851. doi: 10.1021/acs.inorgchem.1c02851.

[17] Jochen Friedrich, Cäcilia Maichle-Mössmer, and Reiner Anwander. Synthesis and derivatisation of ceric tris(tert-butoxy)siloxides. *Chem. Commun.*, 53:12044–12047, 2017. doi: 10.1039/C7CC06499C. URL http://dx.doi.org/10.1039/C7CC06499C.

[18] Ursula J. Williams, David Schneider, Walter L. Dorfner, Cäcilia Maichle-Mössmer, Patrick J. Carroll, Reiner Anwander, and Eric J. Schelter. Variation of electronic transitions and reduction potentials of cerium(iv) complexes. *Dalton Trans.*, 43: 16197–16206, 2014. doi: 10.1039/C4DT01386G. URL http://dx.doi.org/10.1039/C4DT01386G.

[19] Erin M. Broderick, Peter S. Thuy-Boun, Neng Guo, Carola S. Vogel, Jörg Sut- ter, Jeffrey T. Miller, Karsten Meyer, and Paula L. Diaconescu. Synthesis and characterization of cerium and yttrium alkoxide complexes supported by ferrocene-based chelating ligands. *Inorganic Chemistry*, 50(7):2870–2877, 2011. ISSN 0020-1669. doi: 10.1021/ic102076g. URL https://doi.org/10.1021/ic102076g. doi: 10.1021/ic102076g.

[20] I.K. Igumenov, P.P. Semyannikov, S.V. Belaya, A.S. Zanina, S.I. Shergina, and I.E. Sokolov. New volatile -diketonate complexes of barium with sterically hin- dered methoxy--diketones as precursors for cvd. *Polyhedron*, 15(24):4521–4530, 1996. ISSN 0277-5387. doi: https://doi.org/10.1016/0277-5387(96)00176-3. URL https://www.sciencedirect.com/science/article/pii/0277538796001763.

[21] Pei-Pei Cen, Sheng Zhang, Xiang-Yu Liu, Wei-Ming Song, Yi-Quan Zhang, Gang Xie, and San-Ping Chen. Electrostatic potential determined magnetic dynamics observed in two mononuclear -diketone dysprosium(iii) single-molecule magnets. *Inorganic Chemistry*, 56(6):3644–3656, 2017. ISSN 0020-1669. doi: 10.1021/acs. inorgchem.7b00057. URL https://doi.org/10.1021/acs.inorgchem.7b00057. doi: 10.1021/acs.inorgchem.7b00057.

[22] Anjli Hooda, Anuj Dalal, Kapeesha Nehra, Devender Singh, Sumit Kumar, Ra- jender Singh Malik, and Parvin Kumar. Preparation and optical investigation of green luminescent ternary terbium complexes with aromatic -diketone. *Chemical Physics Letters*, 794:139495, 2022. ISSN 0009-2614. doi: https://doi.org/10.1016/

j.cplett.2022.139495. URL https://www.sciencedirect.com/science/article/pii/S0009261422001622.

[23] Nitin S. Nandurkar, Mayur J. Bhanushali, Dinkar S. Patil, and Bhalchandra M. Bhanage. Synthesis of sterically hindered 1,3-diketones. *Synthetic Communications*, 37(23):4111–4115, 2007. doi: 10.1080/00397910701572803. URL https://doi.org/10.1080/00397910701572803.

[24] L. Claisen. Ueber die einführung von säureradicalen in ketone. *Berichte der deutschen chemischen Gesellschaft*, 20(1):655–657, 1887. doi: https://doi.org/10.1002/cber.188702001150. URL https://chemistry-europe.onlinelibrary.wiley.com/doi/abs/10.1002/cber.188702001150.

[25] Emily J. Hopkins, Sebastian M. Krajewski, Aaron S. Crossman, Franklin D. R. Maharaj, Logan T. Schwanz, and Michael P. Marshak. Group 4 organometallics supported by sterically hindered -diketonates. *European Journal of Inor- ganic Chemistry*, 2020(20):1951–1959, 2020. doi: https://doi.org/10.1002/ejic.202000135. URL https://chemistry-europe.onlinelibrary.wiley.com/doi/abs/10.1002/ejic.202000135.

[26] Joe T. Adams and Charles R. Hauser. The acylation of methyl ketones with aliphatic esters by means of sodium amide. synthesis of -diketones of the type rcoch2cor1. *Journal of the American Chemical Society*, 66(7):1220–1222, 1944. ISSN 0002-7863. doi: 10.1021/ja01235a045. URL https://doi.org/10.1021/ja01235a045. doi: 10.1021/ja01235a045.

[27] George S. Hammond, Derek C. Nonhebel, and Chin-Hua S. Wu. Chelates of -diketones. v. preparation and properties of chelates containing sterieally hindered ligands. *Inorganic Chemistry*, 2(1):73–76, 1963. ISSN 0020-1669. doi: 10.1021/ic50005a021. URL https://doi.org/10.1021/ic50005a021. doi: 10.1021/ic50005a021.

[28] Sebastian M. Krajewski, Aaron S. Crossman, Eser S. Akturk, Tim Suhrbier, Steven J. Scappaticci, Maxwell W. Staab, and Michael P. Marshak. Sterically encumbered -diketonates and base metal catalysis. *Dalton Trans.*, 48:10714– 10722, 2019. doi: 10.1039/C9DT02293G. URL http://dx.doi.org/10.1039/ C9DT02293G.

[29] Zhigang ZHAO, Fukiko KUBOTA, Noriho KAMIYA, and Masahiro GOTO. Selective extraction of scandium from transition metals by synergistic extraction with 2-thenoyltrifluoroacetone and tri-ï¿½nï/ï¿-octylphosphine oxide. *Solvent Extraction Research and Development, Japan*, 23(2):137–143, 2016. doi: 10.15261/serdj.23.137.

[30] Soufiane Mekki, Chien M. Wai, Isabelle Billard, Gilles Moutiers, James Burt, Byunghoon Yoon, Joanna S. Wang, Clotilde Gaillard, Ali Ouadi, and Peter Hesemann. Extraction of lanthanides from aqueous solution by using room-temperature ionic liquid and supercritical carbon dioxide in conjunction. *Chemistry – A European Journal*, 12(6):1760–1766, 2006. doi: https://doi.org/10.1002/chem.200500559. URL https://chemistry-europe.onlinelibrary.wiley.com/doi/abs/10.1002/chem.200500559.

[31] S. I. Weissman. Intramolecular energy transfer the fluorescence of complexes of europium. *The Journal of Chemical Physics*, 10(4):214–217, 1942. doi: 10.1063/1.1723709. URL https://doi.org/10.1063/1.1723709.

[32] Adriana Valore, Elena Cariati, Stefania Righetto, Dominique Roberto, Francesca Tessore, Renato Ugo, Ignazio L. Fragalà, Maria Elena Fragalà, Graziella Malandrino, Filippo De Angelis, Leonardo Belpassi, Isabelle Ledoux-Rak, Khuyen Hoang Thi, and Joseph Zyss. Fluorinated -diketonate diglyme lanthanide complexes as new second-order nonlinear optical chromophores: The role of f electrons in the dipolar and octupolar contribution to quadratic hyperpolarizability. *Jour- nal of the American Chemical Society*, 132(13):4966–4970, 2010. ISSN 0002- 7863. doi: 10.1021/ja101081q. URL https://doi.org/10.1021/ja101081q. doi: 10.1021/ja101081q.

[33] P.S. Peijzel, A. Meijerink, R.T. Wegh, M.F. Reid, and G.W. Burdick. A complete 4fn energy level diagram for all trivalent lanthanide ions. *Journal of Solid State Chemistry*, 178(2):448–453, 2005. ISSN 0022-4596. doi: https://doi.org/10.1016/j.jssc.2004.07.046. URL https://www.sciencedirect.com/science/article/pii/S002245960400427X. f-element Spectroscopy and Coordination Chemistry.

[34] Peter A. Tanner, Chris S. K. Mak, Norman M. Edelstein, Keith M. Murdoch, Guokiu Liu, Jin Huang, Luis Seijo, and Zoila Barandiarán. Absorption and emission spectra of ce3+ in elpasolite lattices. *Journal of the American Chemical Society*, 125(43):13225–13233, 2003. ISSN 0002-7863. doi: 10.1021/ja036659x. URL https://doi.org/10.1021/ja036659x. doi: 10.1021/ja036659x.

[35] Simon Cotton. *Lanthanide and Actinide Chemistry*. John Wiley Sons, 2006.

[36] David R. Yarkony. *Nonadiabatic Derivative Couplings*. John Wiley Sons, Ltd, 2002. ISBN 9780470845011. doi: https://doi.org/10.1002/0470845015.cna007. URL https://onlinelibrary.wiley.com/doi/abs/10.1002/0470845015.cna007.

[37] Renata Reisfeld, Amitava Patra, Gérard Panczer, and M. Gaft. Spectroscopic properties of cerium in sol–gel glasses. *Optical Materials*, 13:81–88, 1999.

[38] Natalia G. Kobylinska, Oksana . Dudarko, Inna V. Melnyk, Gulaim A. Seisenbaeva, and Vadim G. Kessler. Luminescence performance of cerium(iii) ions incorporated into organofunctional mesoporous silica. *Microporous and Mesoporous Materials*, 305:110331, 2020. ISSN 1387-1811. doi: https://doi.org/10.1016/j.micromeso. 2020.110331. URL https://www.sciencedirect.com/science/article/pii/S1387181120303346.

[39] Reiner Anwander, Michael Dolg, and Frank T. Edelmann. The difficult search for organocerium(iv) compounds. *Chem. Soc. Rev.*, 46:6697–6709, 2017. doi: 10.1039/C7CS00147A. URL http://dx.doi.org/10.1039/C7CS00147A.

[40] Ian J. Casely, Stephen T. Liddle, Alexander J. Blake, Claire Wilson, and Polly L. Arnold. Tetravalent cerium carbene complexes. *Chem. Commun.*, pages 5037–5039, 2007. doi: 10.1039/B713041D. URL http://dx.doi.org/10.1039/B713041D.

[41] Jean-Claude G. Bünzli and Svetlana V. Eliseeva. Intriguing aspects of lanthanide luminescence. *Chem. Sci.*, 4:1939–1949, 2013. doi: 10.1039/C3SC22126A. URL http://dx.doi.org/10.1039/C3SC22126A.

[42] Jean-Claude G. Bünzli and Claude Piguet. Taking advantage of luminescent lanthanide ions. *Chem. Soc. Rev.*, 34:1048–1077, 2005. doi: 10.1039/B406082M. URL http://dx.doi.org/10.1039/B406082M.

[43] Heather Handl and Robert Gillies. Handl, h.l. gillies, r.j. lanthanide-based luminescent assays for ligand-receptor interactions. life sci. 77, 361-371. *Life sciences*, 77:361–71, 07 2005. doi: 10.1016/j.lfs.2005.01.009.

[44] M. C. Heffern, L. M. Matosziuk, and T. J. Meade. Lanthanide probes for bioresponsive imaging. *Chem Rev*, 114(8):4496–539, 2014. ISSN 0009-2665 (Print) 0009-2665. doi: 10.1021/cr400477t. 1520-6890 Heffern, Marie C Matosziuk, Lauren M Meade, Thomas J U54CA151880/CA/NCI NIH HHS/United States R01EB005866/EB/NIBIB NIH HHS/United States P30 CA060553/CA/NCI NIH HHS/United States U54 CA151880/CA/NCI NIH HHS/United States R01 EB014806/EB/NIBIB NIH HHS/United States R01 EB005866/EB/NIBIB NIH HHS/United States Journal Article Research Support, N.I.H., Extramural Research Support, U.S. Gov't, Non-P.H.S. Review 2013/12/18 Chem Rev. 2014 Apr 23;114(8):4496-539. doi: 10.1021/cr400477t. Epub 2013 Dec 13.

[45] Guochen Bao. Lanthanide complexes for drug delivery and therapeutics. *Journal of Luminescence*, 228:117622, 2020. ISSN 0022-2313. doi: https://doi.org/10.1016/j.jlumin.2020.117622. URL https://www.sciencedirect.com/science/article/pii/S0022231320315891.

[46] Marvin D. Rausch, Kevin J. Moriarty, Jerry L. Atwood, James A. Weeks, William E. Hunter, and Harry G. Brittain. Synthetic, x-ray structural and photoluminescence studies on pentamethylcyclopentadienyl derivatives of lanthanum, cerium and praseodymium. *Organometallics*, 5(6):1281–1283, 1986. ISSN 0276-7333. doi: 10.1021/om00137a048. URL https://doi.org/10.1021/om00137a048. doi: 10.1021/om00137a048.

[47] Marisa J. Monreal, Robert K. Thomson, Thibault Cantat, Nicholas E. Travia, Brian L. Scott, and Jaqueline L. Kiplinger. Ui4(1,4-dioxane)2, [ucl4(1,4-dioxane)]2, and ui3(1,4-dioxane)1.5: Stable and versatile starting materials for low- and high-valent uranium chemistry. *Organometallics*, 30(7):2031–2038, 2011. ISSN 0276-7333. doi: 10.1021/om200093q. URL https://doi.org/10.1021/om200093q. doi: 10.1021/om200093q.

[48] Lars Hirneise, Cäcilia Maichle-Mössmer, and Reiner Anwander. Pentamethylcyclopentadienyl complexes of cerium(iv): Synthesis, reactivity, and electrochemistry. *Inorganic Chemistry*, 60(23):18211–18224, 2021. doi: 10.1021/acs.inorgchem.1c02851. URL https://doi.org/10.1021/acs.inorgchem.1c02851. PMID: 34779192.

[49] Hero J. Heeres, Jaap Renkema, Martin Booij, Auke Meetsma, and Jan H. Teuben. Bis(pentamethylcyclopentadienyl) complexes of cerium(iii). crystal structure of (c5me5)2cech(sime3)2. *Organometallics*, 7(12):2495–2502, 1988. ISSN 0276-7333. doi: 10.1021/om00102a011. URL https://doi.org/10.1021/om00102a011. doi: 10.1021/om00102a011.

[50] Muhammet Köse, Eyup Akgün, and Gökhan Ceyhan. Synthesis, characterization, x-ray structure and photoluminescence properties of two ce(iii) complexes derived from pentadentate ligands. *Journal of Molecular Structure*, 1101:33–40, 2015. ISSN 0022-2860. doi: https://doi.org/10.1016/j.molstruc.2015.08.016. URL https://www.sciencedirect.com/science/article/pii/S0022286015302040.

[51] Haolin Yin, Patrick J. Carroll, Jessica M. Anna, and Eric J. Schelter. Luminescent ce(iii) complexes as stoichiometric and catalytic photoreductants for halogen atom abstraction reactions. *Journal of the American Chemical Society*, 137(29):9234–9237, 2015. ISSN 0002-7863. doi: 10.1021/jacs.5b05411. URL https://doi.org/10.1021/jacs.5b05411. doi: 10.1021/jacs.5b05411.

[52] Marvin D. Rausch, Kevin J. Moriarty, Jerry L. Atwood, James A. Weeks, William E. Hunter, and Harry G. Brittain. Synthetic, x-ray structural and photoluminescence studies on pentamethylcyclopentadienyl derivatives of lanthanum,

cerium and praseodymium. *Organometallics*, 5(6):1281–1283, 1986. ISSN 0276-7333. doi: 10.1021/om00137a048. URL https://doi.org/10.1021/om00137a048. doi: 10.1021/om00137a048.

[53] Paulette N. Hazin, Joseph W. Bruno, and Harry G. Brittain. Luminescence spectra of a series of cerium(iii) halides and organometallics. probes of bonding properties using 4f-5d excited states. *Organometallics*, 6(5):913–918, 1987. ISSN 0276-7333. doi: 10.1021/om00148a002. URL https://doi.org/10.1021/om00148a002. doi: 10.1021/om00148a002.

[54] William J. Evans, John T. Leman, Joseph W. Ziller, and Saeed I. Khan. Synthesis and reactivity of organosamarium diarylpnictide complexes: cleavage reactions of group 15 ee and ec bonds by samarium(ii). *Inorganic Chemistry*, 35(15):4283–4291, 1996. ISSN 0020-1669. doi: 10.1021/ic951627z. URL https://doi.org/10.1021/ic951627z. doi: 10.1021/ic951627z.

[55] William J. Evans. Organometallic lanthanide chemistry. volume 24 of *Advances in Organometallic Chemistry*, pages 131–177. Academic Press, 1985. doi: https://doi.org/10.1016/S0065-3055(08)60415-3. URL https://www.sciencedirect.com/science/article/pii/S0065305508604153.

[56] Herbert Schumann, Juliane A. Meese-Marktscheffel, and Lothar Esser. Synthesis, structure, and reactivity of organometallic .pi.-complexes of the rare earths in the oxidation state ln3+ with aromatic ligands. *Chemical Reviews*, 95(4):865–986, 1995. ISSN 0009-2665. doi: 10.1021/cr00036a004. URL https://doi.org/10.1021/cr00036a004. doi: 10.1021/cr00036a004.

[57] J. M. Birmingham and G. Wilkinson. The cyclopentadienides of scandium, yttrium and some rare earth elements. *Journal of the American Chemical Society*, 78(1): 42–44, 1956. ISSN 0002-7863. doi: 10.1021/ja01582a009. URL https://doi.org/10.1021/ja01582a009. doi: 10.1021/ja01582a009.

[58] Herbert Schumann, Ilse Albrecht, Joerg Loebel, Ekkehardt Hahn, M. Bilayet Hossain, and Dick Van der Helm. Organometallic compounds of the lan- thanides. 36. bis(pentamethylcyclopentadienyl) halide and alkyl derivatives of the lanthanides. *Organometallics*, 5(7):1296–1304, 1986. ISSN 0276-7333. doi: 10.1021/om00138a003. URL https://doi.org/10.1021/om00138a003. doi: 10.1021/om00138a003.

[59] Robert J. Ward, Steven P. Kelley, Wayne W. Lukens, and Justin R. Walensky. Reduction of co2 and cs2 with uranium(iii) metallocene aryloxides. *Organometallics*, 41(12):1579–1585, 2022. ISSN 0276-7333. doi: 10.1021/acs.

organomet.2c00208. URL https://doi.org/10.1021/acs.organomet.2c00208.
doi: 10.1021/acs.organomet.2c00208.

[60] Andrew C. Behrle, Jessica R. Levin, Jee Eon Kim, Jonathan M. Drewett, Charles L. Barnes, Eric J. Schelter, and Justin R. Walensky. Stabilization of miv = ti, zr, hf, ce, and th using a selenium bis(phenolate) ligand. *Dalton Trans.*, 44:2693–2702, 2015. doi: 10.1039/C4DT01798F. URL http://dx.doi.org/10.1039/C4DT01798F.

[61] U. J. Williams, P. J. Carroll, and E. J. Schelter. Synthesis and analysis of a family of cerium(iv) halide and pseudohalide compounds. *Inorg Chem*, 53(12):6338–45, 2014. ISSN 0020-1669. doi: 10.1021/ic500969r. 1520-510x Williams, Ursula J Carroll, Patrick J Schelter, Eric J Journal Article United States 2014/05/31 Inorg Chem. 2014 Jun 16;53(12):6338-45. doi: 10.1021/ic500969r. Epub 2014 May 29.